

Small-molecule inhibitors of the PDZ domain of Dishevelled proteins interrupt Wnt signalling

Nestor Kamdem ^{1,2}, Yvette Roske ³, Dmytro Kovalsky ^{4,6}, Maxim O. Platonov ^{4,6}, Oleksii Balinskyi ^{4,6}, Annika Kreuchwig ^{1,2}, Jörn Saupe ^{1,2}, Liang Fang ^{2,3}, Anne Diehl ¹, Peter Schmieder ¹, Gerd Krause ¹, Jörg Rademann ^{1,5}, Udo Heinemann ^{2,3}, Walter Birchmeier ³ and Hartmut Oschkinat ^{1,2}.

¹ Leibniz-Forschungsinstitut für Molekulare Pharmakologie, Robert-Rössle-Straße 10, 13125 Berlin, Germany

² Institut für Chemie und Biochemie, Freie Universität Berlin, Takustraße 3, 14195 Berlin, Germany

³ Max-Delbrück-Center for Molecular Medicine, Robert-Rössle-Straße 10, 13125 Berlin, Germany

⁴ Enamine Ltd., Chervonotkatska Street 78, Kyiv 02094, Ukraine

⁵ Institut für Pharmazie, Freie Universität Berlin, Königin-Luise-Straße 2 + 4, 14195 Berlin, Germany

⁶ Taras Shevchenko National University, 62 Volodymyrska, Kyiv 01033, Ukraine

Correspondence to: Hartmut Oschkinat (oschkinat@fmp-berlin.de)

Abstract

Dishevelled (Dvl) proteins are important regulators of the Wnt signalling pathway, interacting through their PDZ domains with the Wnt receptor Frizzled. Blocking the Dvl PDZ/Frizzled interaction represents a potential approach for cancer treatment, which stimulated the identification of small molecule inhibitors, among them the anti-inflammatory drug Sulindac and Ky-02327. Aiming to develop tighter binding compounds without side effects, we investigated structure-activity relationships of sulfonamides. X-ray crystallography showed high complementarity of anthranilic acid derivatives in the GLGF loop cavity and space for ligand growth towards the PDZ surface. Our best binding compound inhibits Wnt signalling in a dose-dependent manner as demonstrated by TOP-GFP assays ($IC_{50} \sim 50 \mu M$), and Western blotting of β -catenin levels. Real-time PCR showed reduction in the expression of Wnt-specific genes. Our compound interacted with Dvl-1 PDZ ($K_D = 2.4 \mu M$) stronger than Ky-02327 and may be developed into a lead compound interfering with the Wnt pathway.

KEYWORDS: Drug Design, NMR, PDZ, Frizzled, Wnt signalling

34 INTRODUCTION

35 Dishevelled (Dvl) proteins comprise 500 to 600 amino acids and contain three conserved domains: an
36 N-terminal DIX (**D**ishevelled/**A**xin) domain (Schwarz-Romond 2007, Madrzak 2015), a central PDZ
37 (**P**SD95/**D**lg1/**Z**O-1) domain (Doyle 1996, Ponting 1997), and a C-terminal DEP (**D**ishevelled/**E**gl-
38 10/**P**leckstrin) domain (Wong 2000, Wallingford 2005). Dvl transduces Wnt signals from the membrane
39 receptor Frizzled to downstream components *via* the interaction between Dvl PDZ and Frizzled (Wong
40 2003), thus it has been proposed as drug target (Klaus 2008, Holland 2013, Polakis 2012). Several
41 studies identified internal peptides of the type (KTXXXW) as well as C-terminal peptides of the type
42 ($\Omega\Phi$ GW Φ) in which Ω is any aromatic amino acid (F, W or Y) as Dvl PDZ targets (Lee 2009, Zhang
43 2009). Three Dvl homologues, Dvl-1, Dvl-2 and Dvl-3, have been identified in humans. Sequence
44 identity is 88% between Dvl-3 PDZ and Dvl-1 PDZ and 96% between Dvl-3 PDZ and Dvl-2 PDZ
45 (Supporting Information Figure S1). Dvl proteins are found to be upregulated in breast, colon, prostate,
46 mesothelium, and lung cancers (Weeraratna 2002, Uematsu 2003, Bui 1997, Mizutani 2005).

47 PDZ domains appear in 440 copies spread over more than 260 proteins of the human proteome (Ponting
48 1997). They maintain relatively specific protein-protein interactions and are involved, for example, in
49 signalling pathways, membrane trafficking and in the formation of cell-cell junctions (Zhang 2003,
50 Fanning 1996, Kurakin 2007). Hence, they are potentially attractive drug targets (Rimbault 2019,
51 Christensen 2020). PDZ domains consist of about 90 amino acids which fold into two α -helices and six
52 β -strands exposing a distinct peptide-binding groove (Doyle 1996), Lee 2017). The conserved
53 carboxylate-binding loop (GLGF loop, FLGI in Dvl-2 and -3, Figure 1) is essential for the formation of
54 a hydrogen bonding network between the PDZ domain and PDZ-binding, C-terminal peptide motifs, in
55 most cases coordinating the C-terminal carboxylate group of the interaction partner. In the respective
56 complexes, the C-terminal residue of the ligand is referred to as P₀; subsequent residues towards the N-
57 terminus are termed P₋₁, P₋₂, and P₋₃ etc. Previous studies have revealed that P₀ and P₋₂ are most critical
58 for PDZ-ligand recognition (Songyang 1997, Schultz 1998).

59 PDZ domains are divided into at least three main classes on the basis of their amino acid preferences at
60 these two sites: class I PDZ domains recognize the motif S/T-X- Φ -COOH (Φ is a hydrophobic residue
61 and X any amino acid). Class II PDZ domains recognize the motif Φ -X- Φ -COOH, whereas class III

62 PDZ domains recognize the motif X-X-COOH. However, some PDZ domains do not fall into any of
63 these specific classes (Pawson 2007, Sheng 2001, Zhang 2003). The Dvl PDZ domains, for example,
64 recognize the internal sequence (KTXXXW) within the frizzled peptide 525(GKTLQSWRRFYH)536
65 ($K_D \sim 10 \mu\text{M}$) (Wong 2003, Chandanamali 2009).

66 Due to their occurrence in important proteins, PDZ domains received early attention as drug targets,
67 nicely summarized in Christensen 2019. There are several examples of Dvl PDZ inhibitors of peptide
68 or peptidomimetic nature (eg. Hammond 2006, Haugaard-Kedstrom 2021), including peptide conjugates
69 (eg. Qin 2021, Hegedus 2021), and on an organic, small-molecule basis. The latter approach is
70 considered most beneficial in long term medical treatments of conditions like cancer or neurological
71 disorders. NSC668036 (Shan 2005, Wang 2015) is a peptide-mimic compound which interferes with
72 Wnt signalling at the Dvl level. Based on a computational pharmacophore model of NCS668036,
73 additional compounds were later reported (Shan 2012). Known as first non-peptide inhibitor, the 1H-
74 indole-5-carboxylic acid derivative FJ9 (Fujii 2007) showed therapeutic potential. Further examples
75 including Sulindac (Lee 2009), 2-((3-(2-Phenylacetyl)amino)benzoyl)amino)benzoic acid (3289-8625,
76 also called CalBioChem(CBC)-322338) (Grandy 2009, Hori 2018), N-benzoyl-2-amino-benzoic acid
77 analogs (Hori 2018), phenoxyacetic acid analogs (Choi 2016), and Ethyl 5-hydroxy-1-(2-oxo-2-((2-
78 (piperidin-1-yl)ethyl)amino)ethyl)-1H-indole-2-carboxylate (KY-02327) (Kim 2016) have been
79 reported, with the latter showing the highest *in-vitro* affinity ($8.3 \mu\text{M}$) of all. Despite the existence of the
80 abovementioned inhibitors of Dvl PDZ, the development of tighter-binding, non-peptidic small-
81 compound modulators of the respective functions, binding with nanomolar affinity, is necessary and
82 remains challenging. On this path, we explore optimal fits for the primary binding pocket by cycles of
83 chemical synthesis and X-ray crystallography and further avenues for systematically growing ligands
84 along the Dvl PDZ surface to provide SAR for the development of inhibitors in the low or medium
85 nanomolar range. Nuclear magnetic resonance (NMR) spectroscopy was used to detect primary hits and
86 for follow-up secondary screening. The ability of NMR to detect weak intermolecular interactions (μM
87 $< K_D < \text{mM}$) make it an ideal screening tool for identifying and characterizing weakly binding fragments,
88 to be optimized subsequently by chemical modification in order to improve binding (Zartler 2006,
89 Shuker 1996, Zartler 2003). Besides NMR, the determination of X-ray crystal structures of selected

90 complexes was fundamental for further design of new compound structures with improved binding. In
91 the first round of screening, a library constructed after computational docking of candidates into the
92 peptide binding site of the Dvl PDZ domains were investigated, followed by secondary screening
93 utilizing a library of 120 compounds containing rhodanine or pyrrolidine-2,5-dione moieties.

94

95 **RESULTS AND DISCUSSION**

96 **PDZ targeted library design**

97 The PDZ targeted library was designed to cover all PDZ domains with available structure. For this, all
98 X-ray and NMR derived PDZ structures were retrieved from the PDB, clustered, and 6 selected centroids
99 were subjected to the virtual screening routine. The area considered is shown in Figure 1A, with the blue
100 sphere indicating the geometrical centre. The clustering of the PDZ domains was performed according
101 to the shapes of their binding sites, rather than backbone conformation. This approach accounts for the
102 importance of surface complementarity of protein-small molecule interactions and the critical
103 contribution of van der Waals interactions to the binding free energy. On another hand, PDZ domains
104 have evolved to recognize a carboxyl group that is mostly derived from the C-terminus of natively
105 binding proteins. Finally, the fact that PDZ can recognize internal motifs (Hillier 1999), including
106 KTXXXW of Frizzled-7 recognised by Dvl PDZ (Wong 2003, Chandanamali 2009), raises the question
107 of what are key binding contributions with PDZ domains: negative charge, hydrogen bonding or shape
108 complementarity (Harris 2003). For this reason, tangible compounds were preselected to have extensive
109 hydrophobic contacts as well as chemical groups that mimic the carboxylic group.

110 Virtual screening was performed with QXP, and the generated complexes were sequentially filtered with
111 a self-designed MultiFilter algorithm. From the resulting 1119 compounds a randomly selected set of
112 250 compounds was subjected to NMR validation.

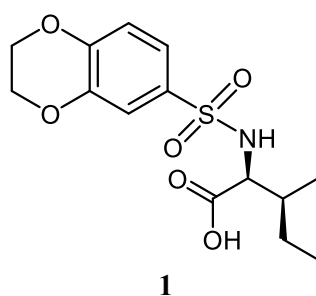
113

114 **NMR Screening and development of compounds**

115 The results of virtual screening were checked experimentally by comparing 2D ¹H-¹⁵N HSQC
116 (Heteronuclear Single Quantum Correlation) spectra of Dvl-3 PDZ in the absence and presence of the
117 compound to elucidate ligand-induced changes of chemical shifts. Chemical shift perturbation

118 differences (ΔCSP , representing the average of the three strongest shifting cross peaks according to
119 equation 1) were evaluated in cases where the residues responding strongest are inside the area defined
120 by Figure 1A. The responses were classified into: (i) inactive compounds ($\Delta\text{CSP} < 0.02$); (ii) very weak
121 interactions ($0.02 \leq \Delta\text{CSP} \leq 0.05$); (iii) weak interactions ($0.05 < \Delta\text{CSP} \leq 0.1$); (iv) intermediate
122 interactions ($0.1 < \Delta\text{CSP} \leq 0.2$); (v): strong interactions ($0.2 < \Delta\text{CSP} \leq 0.5$) and (vi) very strong
123 interactions ($\Delta\text{CSP} > 0.5$). In most cases, the signals of residues S263, V287 and R320 (Figure 1A)
124 within the conserved binding site were most strongly perturbed (Supporting Information Figure S2).
125 With the ΔCSP of 0.12 ppm, the isoleucine-derived compound **1** ((2,3-dihydrobenzo[b][1,4]dioxin-6-
126 yl)sulfonyl)-L-isoleucine containing a sulfonamide moiety was detected initially as one of the best “hits”
127 according to chemical shift changes. The sulfonamide is a well-known moiety in drug discovery
128 (Mathvink 1999, Wu 1999, Sleight 1998 O’Brien 2000, Tellew 2003).

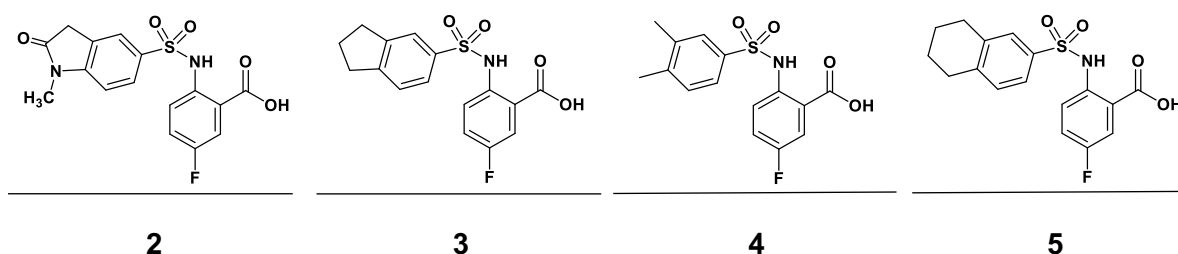
129



130
131

132 Upon NMR titration experiments for compound **1** (Supporting Information Figure S2) with Dvl-3 PDZ,
133 the largest chemical shift perturbations were observed for S263 in strand βB and R320 in helix αB of
134 Dvl-3 PDZ, confirming the conserved binding site.

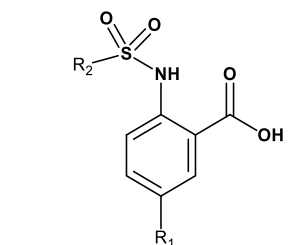
135



136 **Scheme 1:** Compounds **2**, **3**, **4**, **5**

137 By comparing the binding of several sulfonamide compounds in a secondary screening event and mak-
138 ing use of our in-house library, four new compounds (**2**, **3**, **4**, **5**) that induced chemical shift perturbations
139 larger than 0.2 ppm were found (for binding constants see Table 1) and considered further as reasonably

140 strong binders. The similarity of the structures led us to define Scheme 2 as a scaffold for further refine-
141 ments. Sulfonamides were considered more drug-like, and hence followed up at higher priority than
142 other hits. We realised that our four new compounds had different moieties at R₂ in combination with a
143 small R₁ (fluorine). A decrease of binding was observed with decreasing size of R₂.

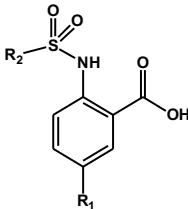
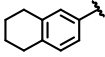
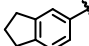
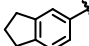
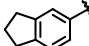
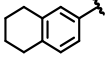
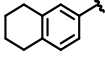
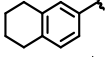
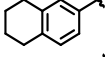
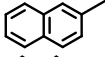
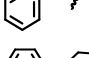
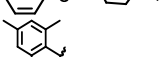
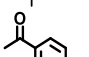
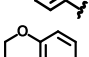
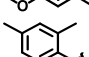
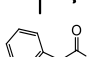
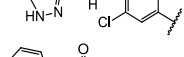
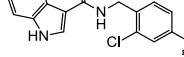
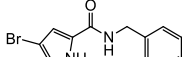
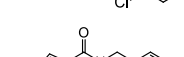


144 **Scheme 2:** Basic fragment for further synthesis

145 In order to assess the importance of the aryl group at R₂ for complex formation, it was replaced by a
146 methyl group as substituent to yield compound **6**, which showed a drastic decrease of binding (Table 1).
147 Compounds **3**, **4**, and **5** did not distinguish between the Dvl-3 PDZ and Dvl-1 PDZ. In order to obtain
148 detailed insight into the binding mode of these compounds, crystal structures of Dvl-3 PDZ in complex
149 with compounds **3**, **5** and **6** were determined (Figure 1). For compound **3** the crystal structure revealed
150 two complexes within the crystallographic asymmetric unit (AU) at 1.43 Å resolution. Both show the
151 anthranilic acid with the attached fluorine pointing into the hydrophobic binding pocket (Figure 1B and
152 Supporting Information Figure S3A), while the carboxyl group forms a hydrogen-bond network with
153 amide residues of the carboxylate binding loop, in particular strand βB (Figure 1B) and specifically with
154 residues I262, G261 and L260. The two sulfonamide oxygen atoms form hydrogen bonds with R320
155 and H324 (weak) of helix αB for only one complex in the AU. The aromatic aryl group
156 (tetrahydronaphtalene) attached to the sulfonamide is involved in hydrophobic interactions with F259
157 (Supporting Information Figure S3B). The 1.6-Å complex structure with compound **5** (4 molecules per
158 AU) exhibits a comparable binding mode as found for compound **3** with a hydrogen-bond network
159 involving the carboxyl group and the amides of I262, G261, L260, and of the sulfonamide to H324
160 (Figure 1C). No hydrogen bond was observed to R320 in all four molecules of the AU, but small
161 variations of the aryl moiety relative to F259 (Supporting Information Figure S3C). The crystals of the
162 complex with **6** show two molecules in the AU (Figure 1D). The sulfonamide is bound by H324 in both

163 complexes (Supporting Information Figure S3D). However, compound **6** bound only in the mM range
 164 as compared to **3** and **5**, which obviously results from the missing aromatic rings.

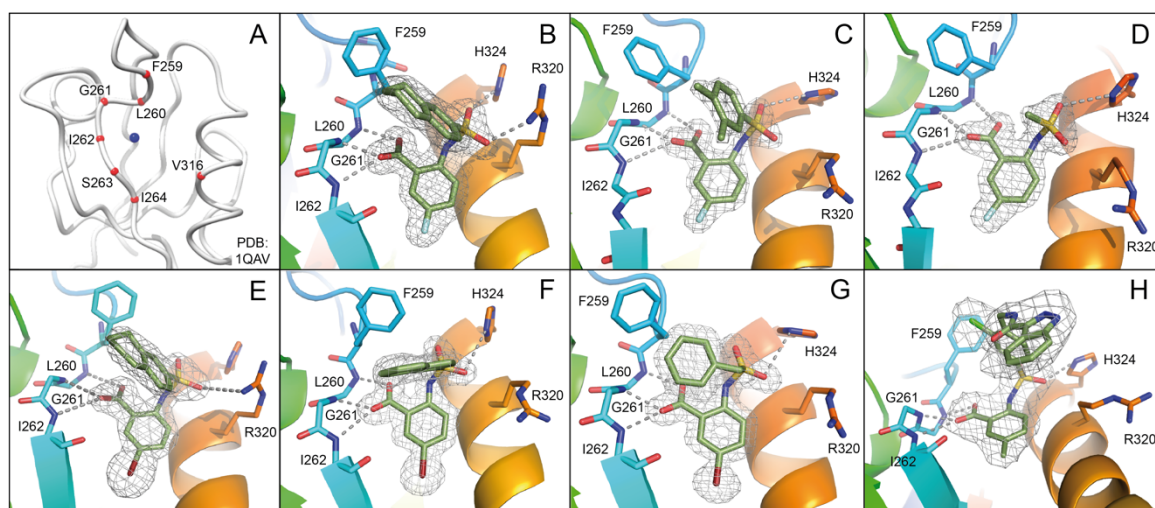
165

	ID	R ₁	R ₂	(K _D , μM) Dvl-3PDZ	(K _D , μM) Dvl-1 PDZ
	2	F		nd	237.6 ± 38.5 ^{NMR}
	3	F		80.6 ± 6.1 ^{NMR}	112.7 ± 25.9 ^{NMR}
	4	F		83.9 ± 7.8 ^{NMR}	114.4 ± 9.8 ^{NMR}
	5	F		140.6 ± 14.1 ^{NMR}	160.1 ± 14.6 ^{NMR}
	6	F	CH ₃	> 1000 ^{ITC}	-
	7	Br		20.6 ± 2.4 ^{NMR}	18.2 ± 2.4 ^{NMR}
	8	CF ₃		17.4 ± 0.5 ^{ITC}	24.5 ± 1.5 ^{ITC}
	9	Cl		41.1 ± 3.1 ^{NMR}	45.6 ± 4.5 ^{NMR}
	10	CH ₃		62.5 ± 4.7 ^{NMR}	60.5 ± 5.3 ^{NMR}
	11	Br		13.8 ^{ITC}	119.9 ^{ITC}
	12	Br		58.5 ^{ITC}	nd
	13	Br		7.2 ^{ITC}	213.2 ^{ITC}
	14	Br		58.1 ± 2.1 ^{ITC}	nd
	15	CF ₃		52.9 ± 1.7 ^{ITC}	nd
	16	CF ₃		59.1 ± 1.5 ^{ITC}	nd
	17	CF ₃		49.5 ^{ITC}	nd
	18	CH ₃		9.4 ± 0.6 ^{ITC}	2.4 ± 0.2 ^{ITC}
	19	CH ₃		21.8 ± 1.7 ^{ITC}	8.0 ± 0.5 ^{ITC}
	20	CH ₃		9.8 ± 0.3 ^{ITC}	4.7 ± 0.3 ^{ITC}
	21	CH ₃		12.5 ± 0.5 ^{ITC}	4.7 ± 0.2 ^{ITC}

166
 167

168 **Table 1.** Binding constants K_D (μM) of Dvl-3 PDZ and Dvl-1 PDZ for compounds 3 – 21 derived by ITC or NMR if not
 169 specified. The K_D values determined by NMR are reported as means ± standard deviations of measurements evaluating shifts
 170 of cross peaks of at least six residues influenced upon binding of the ligand. The K_D values (1/K_A) determined by ITC were
 171 obtained as fits to a one-site binding model (n in the range of 0.95-1.2) with K_D errors obtained by ΔK_A/K_A².

172



173
 174 **Figure 1:** A Definition of PDZ binding site. The center of the binding site (blue sphere) is defined as the geometric center of
 175 $\text{C}\alpha$ atoms (red spheres) of 7 residues (typed in red) defined by multiple sequence alignment. **B-H** Magnified views into crystal
 176 structures of various compounds bound to the Dvl-3 PDZ domain. The 2Fo-Fc electron density around the compounds is shown
 177 at 1σ contour level, and the dotted lines indicate formed hydrogen bonds. In the bound compounds covalent bonds to carbon
 178 atoms are shown as green sticks. Important residues involved in compound binding are labelled and displayed in atom colours
 179 (carbons blue or dark yellow). **B-D** show compound **3**, **5** and **6** respectively. All compounds in **B-D** contain fluorine (light
 180 blue) in para position to the amine. **E-G** represents the bound compounds **7**, **11** and **12**, respectively. All have bromine (dark
 181 red) in para position to the amine. **H** shows compound **18** within the binding site. The accession codes of the structures B-H
 182 are 6ZBQ, 6ZBZ, 6ZC3, 6ZC4, 6ZC6, 6ZC7 and 6ZC8, respectively.

183
 184 To further explore the importance of the fluorine site inside the hydrophobic pocket, substitutions by
 185 bromine, chlorine, methyl and trifluoromethyl were chosen. In fact, the methyl group has a similar vdW
 186 radius as the CF_3 group. Iodine was not considered a good candidate since it increases molecular weight
 187 substantially and the compounds may be chemically less stable, in particular in biological assays. Taking
 188 into account that compound **6** did not bind because of the missing aromatic ring at the R_2 position, our
 189 overall strategy was to increase the aromatic ring at R_2 while finding a good fit for R_1 , keeping an eye
 190 on the molecular weight to enable further compound modifications that fulfil key properties as defined
 191 by Lipinski (Lipinski 2000, Lipinski 1997). Our preference to continue exploration at the R_1 position of
 192 the aromatic ring in Scheme 1 was inspired by the absence of hits with other substitutions in the
 193 secondary screening event and the initial X-ray structures that showed a hydrophobic pocket available
 194 for substituents in this position while other sites at the aromatic ring would include steric hindrance.
 195 Therefore, compounds **7-17** were obtained and were classified in three different groups to derive
 196 structure activity relationships (SAR). The compounds **7-10** in group 1 contain different R_1 (Br, CF_3 ,
 197 Cl, CH_3) but the same moiety (tetrahydronaphthalene) at R_2 . As expected, binding could be further
 198 improved by displacement of the fluorine with elements exhibiting larger van der Waals (vdW) radii.

199 Indeed, the K_D decreased stepwise and the best fit was observed for compound **8** containing a
200 trifluoromethyl group ($K_D = 17.4 \mu\text{M}$ for Dvl-3 PDZ and $24.5 \mu\text{M}$ for Dvl-1 PDZ). The different
201 substituents at the R_1 position contribute to an increased binding affinity in the following order: $F < Cl$
202 $< Br < CF_3$ (compound **3** $< \mathbf{9} < \mathbf{7} < \mathbf{8}$, respectively). Compound **10** with a methyl group at the R_1 position
203 showed only marginally improved binding, although the methyl group has a similar vdW radius as the
204 CF_3 group of compound **8**. The difference in binding results most likely from their different
205 hydrophobicity.

206 The 1.85-Å crystal structure of the Dvl-3 PDZ domain with compound **7** ($K_D = 20.6 \mu\text{M}$ for Dvl-3 PDZ
207 and $18.2 \mu\text{M}$ for Dvl-1 PDZ) showed an identical hydrogen-bond network involving the amide groups
208 of residues I262, G261 and L260 of the carboxyl binding loop as seen for all other complex structures
209 reported here (Figure 1E). Only one hydrogen bond between the sulfonamide and R320 was found in
210 addition for one of the two Dvl-3 PDZ molecules per AU. H324 of Dvl-3 PDZ was not addressed by the
211 sulfonamide as seen previously. The bromine at position R_1 points into the hydrophobic pocket, similar
212 as the fluorine in the complex structure with compound **3**. The two complexes in the AU show significant
213 variations in the positions of the tetrahydronaphthalene rings as well as for the side chain of F259 and
214 R320 (Supporting Information Figure S3E).

215 Following the analysis of the complex involving compound **7**, the binding characteristics of the group-
216 2 compounds (**11-14**) were investigated. They contain bromine as R_1 and different substituents at the R_2
217 position to assess the importance of π - π stacking interactions involving F259. K_D values of $7.2 \mu\text{M}$ for
218 compound **13** and $13.8 \mu\text{M}$ for compound **11** were found with respect to the interaction with Dvl-3 PDZ.
219 Crystal structures of Dvl-3 PDZ in complex with compound **11** (1.58 Å resolution, 1 molecule per AU)
220 and **12** (1.48 Å, 2 molecules per AU) revealed very similar binding as observed in the crystal structures
221 with compounds **3** and **7**. The aromatic rings at R_2 show hydrophobic interactions to F259, but not a
222 classical π - π stacking as expected. Nevertheless, the tighter binding of compound **11** could be explained
223 by the larger aromatic substituent at the R_2 position compared to compound **12**. Both complex structures
224 show also non-specifically bound ligands in crystal contacts (Supporting Information Figure S3H,
225 Supporting Information Tables S2 and S3). The additional ligand molecules in both complex structures
226 can be explained as a crystallographic artefact, which is verified with ITC experiments that indicate 1:1

227 stoichiometries in both cases (Figure S5). With respect to the selectivity of the tested compounds we
228 observed a 6 to 30-fold stronger binding of compounds **7**, **9**, **11** and **13** to Dvl-3 PDZ as compared to
229 Dvl-1 PDZ. These differences are related to the different sequences at the end of α B. Most importantly,
230 H324 is replaced by a serine residue in the Dvl-1 PDZ domain.

231 The group-3 compounds (**15-17**) contain a trifluoromethyl at position R_1 and were tested to investigate
232 a cooperative role of this moiety with various substituents at position R_2 . All compounds bind weaker
233 to Dvl-1 and Dvl-3 than compound **8** which contains tetrahydronaphthalene at the R_1 position, revealing
234 its important role in the interaction.

235

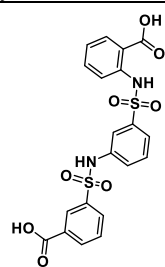
236 **Further modifications towards higher affinity and reduced toxicity**

237 Possible cytotoxic effects of compounds **3**, **7**, **8**, **9**, and **10** were evaluated in cell viability assays using
238 HEK293 cells (Supporting Information Figure S4). These compounds were selected due to different
239 substituents at the R_1 , including halogens. Cell viability was measured 24h after treatment with the
240 individual compounds, and half maximal inhibitory concentrations (EC_{50}) were calculated for each
241 compound. The compounds exhibited EC_{50} values in the range of 61-131 μ M (Supporting Information
242 Figure S4A). Compounds **3** and **10** that contained fluorine or methyl group substituents at R_2 ,
243 respectively, were the least toxic, while compound **7**, containing bromine, was the most toxic. The
244 results from crystallography, modelling studies and of the cell proliferation assays led us to further
245 investigate compounds **18-21** that contain a methyl group at the R_1 position and different substituents
246 as R_2 . In this way, we aimed to develop both potent and less toxic, cell permeable inhibitors. All
247 compounds showed strong interactions as indicated by chemical shift perturbation values between 0.30
248 to 0.34 ppm (Supporting Information Table S1). The binding constants were evaluated by ITC whereby
249 compound **18** ($K_D = 9.4 \mu$ M for Dvl-3 PDZ and 2.4μ M for Dvl-1 PDZ) appeared to be most potent.
250 Compound **18** contains a pyrazole ring which is considered as an important biologically active
251 heterocyclic moiety (Lv 2010). Compounds **20** ($K_D = 9.8 \mu$ M for Dvl-3 PDZ and 4.7μ M for Dvl-1 PDZ)
252 and **21** ($K_D = 12.5 \mu$ M for Dvl-3 PDZ and 4.7μ M for Dvl-1 PDZ) contain pyrrole rings. Their binding
253 constants almost have the same value despite the different substituents (bromine or chlorine) at the
254 pyrrole rings. The binding of compounds **18-21** to both Dvl PDZ domains is mainly enthalpy-driven as

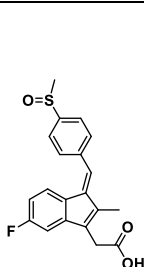
255 indicated in Table 2, with a slightly stronger effect for Dvl-1 PDZ than for Dvl-3 PDZ. To our surprise,
 256 the crystal structure of Dvl-3 PDZ in complex with compound **18** shows the pyrazole substituent in the
 257 R₂ position orientated away from the binding pocket. Instead, a π - π stacking interaction with F259 was
 258 observed (Supporting Information Figure S3I). Cytotoxicity of **18-21** was determined *via* MTT assays
 259 (Mosmann 1983) that displayed viability up to concentrations above 150 μ M (Supporting Information
 260 Figure S4B).

261

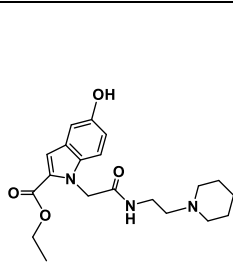
Compound	Dvl-3 PDZ				Dvl-1 PDZ			
	K _D (μ M)	Δ H (kcal/ mol)	T Δ S (kcal/ mol)	Δ G (kcal/ mol)	K _D (μ M)	Δ H (kcal/ mol)	T Δ S (kcal/ mol)	Δ G (kcal/ mol)
18	9.4 \pm 0.6	-8.0	-1.2	-6.8	2.4 \pm 0.2	-12.2	-4.7	-7.5
19	21.0 \pm 1.7	-5.9	0.4	-5.5	8.0 \pm 0.5	-7.3	-0.3	-7.0
20	9.8 \pm 0.3	-10.4	-3.6	-6.8	4.7 \pm 0.3	-9.4	-2.2	-7.2
21	12.5 \pm 0.5	-5.9	0.7	-6.8	4.7 \pm 0.2	-8.5	-1.5	-7.0
NPL-1011	79.7 \pm 53.3							
Sulindac	8.3 \pm 2.5							
CBC-322338/ 3289-8625	> 400 μ M							
NSC668036	> 400 μ M							
Ky-02327					8.3 \pm 0.8 ^{16g}			



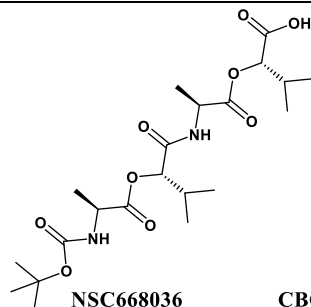
NPL-1011



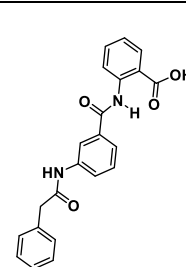
Sulindac



Ky-02327



NSC668036



CBC-322338 / 3289-8625

265

266 **Table 2:** Isothermal titration calorimetric data for the reaction between Dvl-3 PDZ, Dvl-1 PDZ and our compounds **18**, **19**, **20**
 267 and **21** respectively. Compounds NPL-1011 (Hori 2018), and Sulindac (Lee 2009), CBC-322338/3289-8625 (Grandy 2009,
 268 Hori 2018), and NSC668036 (Shan 2005), for more thermodynamic parameters see Supporting Information Figure S7. For Ky-
 269 02327 the value from literature is included.

270

271 Comparison to reported Dvl PDZ-binding molecules

272 Our compounds bind to Dvl-3 with a K_D better than 10 μ M, and slightly tighter to Dvl-1, see Table 2,
 273 with **18** showing a K_D of 2.4 μ M and chemical shift changes indicating binding to the canonical binding
 274 site (Figure 1A). For comparison, four compounds of those shown in Supporting Information Figure S6
 275 were assayed by ITC (Supporting Information Figure S7) regarding their affinity to Dvl-3 PDZ. Ky-
 276 02327 was already determined to bind with a K_D of 8.3 \pm 0.8 μ M (Kim 2016) to Dvl-1 PDZ. Our first
 277 interest was oriented towards sulfonamides. Hori et al (Hori 2018) have recently reported 3-({3-[(2-
 278 carboxyphenyl)sulfamoyl]phenyl}sulfamoyl)benzoic acid (NPL-1011) binding to Dvl-1 PDZ via the

279 detection of chemical shift changes, and further sulfonamide compounds that showed smaller effects,
280 indicating weaker binding. We examined the binding constant of NPL-1011 which possesses two
281 sulfonamide moieties by ITC and found a value of $79.7 \pm 53.3 \mu\text{M}$, see Table 2. For further comparisons,
282 we assayed also CBC-322338/3289-8625, Sulindac and NSC668036 by ITC. Surprisingly, CBC-
283 322338/3289-8625 showed very low affinity, with a K_D above $400 \mu\text{M}$ in our ITC assay, in line with
284 the value found by Hori et al (Hori 2018) ($954 \pm 403 \mu\text{M}$). We also applied an NMR shift assay (Figure
285 S8), yielding a ΔCSP around 0.1. Based on NMR and ITC studies, the binding affinity of CBC-
286 322338/3289-8625 to DVL-3 seems to be less than 50 micromolar (comparing the CSPs from the NMR
287 assay with those of our other compounds listed in Table S1 and the respective binding constants in Table
288 1, and considering also the weak heat development in our ITC assay) which was larger than the originally
289 reported value (10.6 ± 1.7) (Grandy 2009) that was obtained with a different method. Concerning non-
290 sulfonamide compounds, a K_D of $8.3 \pm 2.5 \mu\text{M}$ was detected for Sulindac, while NSC668036 (Shan
291 2005) did not show high-affinity binding. These results are largely in agreement with literature. In all
292 cases, compounds were tested for purity after K_D measurements (see Supporting Information Figures
293 S9A-D).

294

295 **Selectivity testing using a set of selected PDZ domains**

296 Compounds **18**, **20** and **21** were tested towards other PDZ domains for selectivity. The set included
297 PSD95-PDZ 2 and 3, Shank-3, α -syntrophin, and AF-6 PDZ. According to the determined chemical
298 shift perturbations (Supporting Information Table S4), our compounds show no or very weak
299 interactions with the selected PDZ domains ($0.05 < \Delta\text{CSP} \leq 0.1$) ppm. These findings led to the
300 conclusion that our compounds show considerable selectivity towards Dvl PDZ domains. This
301 selectivity might be due to a unique feature of Dvl PDZ where R320 (Dvl-3 PDZ) or R322 (Dvl-1 PDZ)
302 are crucial for interactions, explaining selectivity with respect to other PDZ domains. In addition, the
303 large hydrophobic cavity for the side chain of the C-terminal residue of the interacting peptide is
304 occupied by a large moiety in case of compounds **18**, **20** and **21** which might not be accommodated in
305 most other PDZ domains.

306

307 **Dvl inhibitors antagonize canonical Wnt signalling and Wnt-related properties of cancer cells**

308 Taking advantage of a lentivirus that encodes GFP in a β -catenin/TCF-dependent fashion (TOP-GFP,
 309 SABiosciences), a stable HEK293 reporter cell line was established to evaluate the inhibitory effect of
 310 compounds **18**, **20** and **21** on canonical Wnt signalling activity. TOP-GFP expression in this cell line
 311 was induced by the ligand Wnt3a, which directly activates the Frizzled-Dishevelled complex and
 312 protects β -catenin from degradation by the destruction complex (Figure 2A). Remarkably, all three
 313 compounds inhibited Wnt signalling induced by Wnt3a in a dose-dependent manner (Figure 2B),
 314 yielding IC_{50} values between 50-80 μ M.

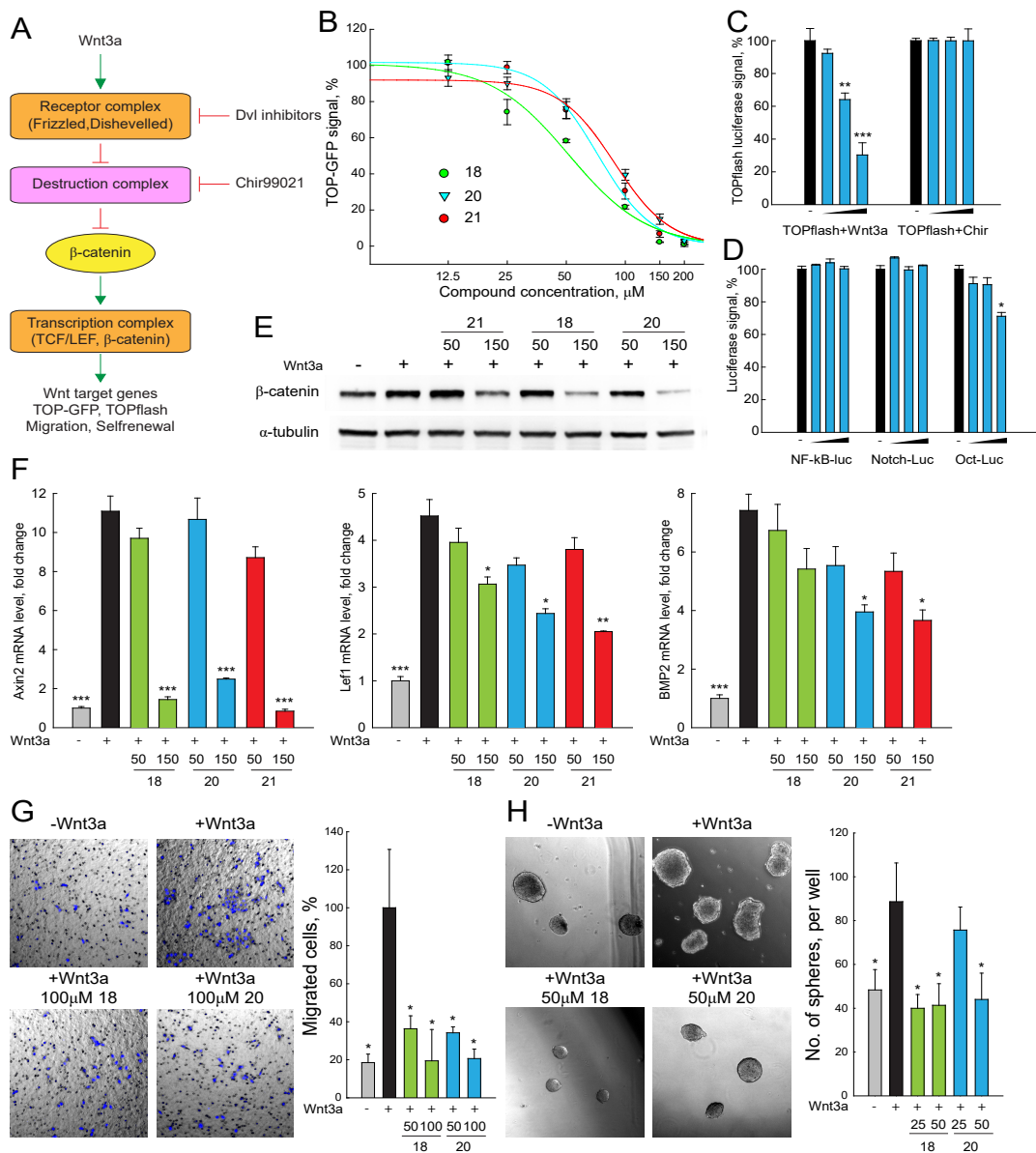


Figure 2

315 **Figure 2.** DVL inhibitors antagonize Wnt signalling and Wnt related properties of cancer cells induced by Wnt3a. A. Scheme
 316 of Wnt signalling pathway. Important components of the Wnt signalling pathway are schematically presented. Wnt3a treatment
 317

318 increases the transcription of Wnt targets, enhances signals of TOP-GFP and TOPflash assays, and promotes Wnt related
319 biological properties of cancer cells. **B.** TOP-GFP reporter assays were performed with HEK293 reporter cell line. Compound
320 **18, 20** and **21** inhibited Wnt3a induced Wnt activation in dose-dependent manner with IC_{50} of 50~75 μ M. **C&D.** TOPflash
321 assays stimulated with Chir99021 and reporter assays of other pathway were used to evaluate the specificity of compound **20**.
322 Compound **20** specifically inhibited Wnt3a induced Wnt activation, and had no or mild effect on Chir99021 induced Wnt
323 activation and other signalling pathways including NF- κ B, Notch and Oct4. **E.** β -Catenin protein levels were detected with
324 Western blotting in Hela cells. Compound **18, 20** and **21** (150 μ M) inhibited accumulation of β -catenin in Hela cells treated
325 with Wnt3a. **F.** The mRNA levels of Wnt target genes (Axin2, Lef1 and Bmp2) in Hela cells were measured with quantitative
326 real-time PCR. Compounds **18, 20** and **21** (150 μ M) reduced the transcription of Wnt target genes that are enhanced by Wnt3a
327 treatment in Hela cells. **G.** Cell migration of SW480 cells after Wnt3a treatment was assessed by transwell assays. Compounds
328 **18** and **20** (50~100 μ M) reduced the migration of SW480 cells enhanced by Wnt3a. **H.** SW480 cells were cultured in serum-
329 free non-adherent condition to evaluate the self-renewal property enhanced by Wnt3a treatment. Compound **18** and **20** (25~50
330 μ M) reduced sphere formation of SW480 cells that was enhanced by Wnt3a treatment. For all tests, three independent
331 biological replicas were performed and error bars represent standard deviations. P-values were calculated from T-test. *: P <
332 0.05; **: P < 0.01; ***: P < 0.001.

333
334

335 To further evaluate the specificity of our Dvl inhibitors, the conventional TOPflash (Molenaar 1996)
336 and other luciferase reporter assays were performed. In Hela cells, **20** inhibited TOP-luciferase signals
337 stimulated by Wnt3a but not by CHIR99021(Sineva 2010), a compound that activates Wnt signalling
338 downstream of Dvl (Figure 2A, C). Compound **20** had no significant inhibitory effects in reporter assays
339 that measure the activity of other signalling systems, e.g., NF- κ B-luciferase stimulated by recombinant
340 TNF α , Notch-luciferase stimulated by the overexpression of the Notch intracellular domain, or the Oct-
341 luciferase assay that is stimulated by overexpression of Oct4 (SABiosciences, Figure 2D). These results
342 strongly indicate that **20** is specific for canonical Wnt signalling at the upstream level.

343 Increased β -catenin protein level is a hallmark of active Wnt signalling (Kishida 1999). Once β -catenin
344 is accumulated in the cytoplasm, it can translocate into the nucleus and activate the transcription of Wnt
345 target genes by interacting with transcription factors of the TCF/LEF family (Figure 2A) (Behrens
346 1996). In Hela cells, all three Dvl inhibitors blocked the increase of production of β -catenin by Wnt3a
347 in dose-dependent manners, as seen by Western blotting (Figure 2E). Increased mRNA levels of the
348 Wnt target genes Axin2, Lef1 and Bmp2 (Riese 1997, Jho 2002, Lewis 2010) were induced by Wnt3a
349 treatment, as measured by qRT-PCR, and these increases were reduced by compounds **18, 20** and **21**
350 (Figure 2F). These results demonstrate that compounds **18, 20** and **21** inhibit Wnt signalling as indicated
351 by reduced accumulation of β -catenin and low expression of typical Wnt target genes.

352 Canonical Wnt signalling contributes to cancer progression by inducing high motility and invasion of
353 cancer cells while retaining the self-renewal property of cancer initiating cells (Fritzmann 2009, Sack
354 2011, Vermeulen 2010, Malanchi 2008). In particular, cancer initiating cells are propagated and
355 enriched in non-adherent sphere culture, demonstrating the self-renewal capacity of the stem cells

356 (Kanwar 2010, Fan 2011). To investigate the potential value of the Dvl inhibitors for interfering with
357 these Wnt-related properties of cancer cells, the subline SW480WL was derived from the SW480 colon
358 cancer cell line, which exhibits a low level of endogenous Wnt activity (Fang 2012). The cell migration
359 and self-renewal properties of SW480WL cells were enhanced by Wnt3a treatment, as revealed by
360 transwell and sphere formation assays (Figure 2G, H). Compounds **18** and **20** prevented increased cell
361 migration and sphere formation. These results indicate that our Dvl inhibitors may be developed into
362 lead compounds that interfere with Wnt signalling.

363

364 **CONCLUSIONS**

365 In the present work, small molecules that bind to Dvl PDZ in the one-digit micromolar range with
366 considerable selectivity have been developed by an extensive structure-based design approach. With
367 regards to the affinity determined by ITC, compound **18** binds to Dvl-1 and Dvl-3 in vitro with K_D values
368 of 2.4 and 9.4, respectively, comparing very well with known ligands. X-ray structures of Dvl-3 PDZ
369 complexes with selected compounds provided insight into crucial interactions and served as the basis
370 for the design of tight binding compounds with reduced toxicity. The structural investigations revealed
371 that these compounds form hydrogen bonds with the amide groups of residues L260, G261 and I262 in
372 the PDZ-domain loop and the side chains of residues H324 and R320. Finally, the chosen methodology,
373 virtual screening followed by a two-stage NMR based screening, X-ray crystallography, and chemical
374 synthesis is an excellent path towards bioactive interaction partners. Our best compounds effectively
375 inhibited the canonical Wnt signalling pathway in a selective manner and could be developed for further
376 studies.

377

378 **Experimental Section**

379 **Clustering binding sites and selection of representative PDZ domains**

380 Three-dimensional structures of PDZ domains were retrieved from the PDB (Berman 2000). At the time
381 of the study from a total of 266 PDB files, 126 were NMR solution structures and 140 derived from X-
382 ray diffraction studies. The structures belong to 163 PDZ domains of 117 different proteins from 11
383 organisms. Files which contain more than one 3D conformation for a domain (up to 50 for NMR-derived

384 data) were split into separate structures and considered independently. The total number of unique 3D
385 structures was 2,708.

386 Amino acid sequences of PDZ domains were aligned using Clustal Omega software (Sievers 2011).
387 Based on the alignment, for each structure, residues which form the binding site (strand β B and helix
388 α B) were determined (Supporting Information Figure S8). The centre of the binding site was defined as
389 a geometric centre of $C\alpha$ atoms of 7 residues (6 residues from the β B strand and the second residue from
390 the α B helix). Such bias toward the β B strand was made to cover sites occupied by residues in -1 and -
391 3 positions.

392 The triangulated solvent accessible surface for each PDZ structure was built using MSMS software
393 (Sanner 1996) with a spherical probe radius of 1.4 Å and vertex density 10 Å⁻¹. The largest connected
394 set of surface vertices within 9 Å from the centre of the binding site was used to construct shape-based
395 numerical descriptors. The descriptors are 508-dimensional vectors of non-negative integer numbers
396 and were built using a shape distributions approach (Osada 2002). In total 10 (Pawson 2007) vertex
397 triplets were selected randomly, each forming a triangle. Triangles which had a side longer than 16 Å
398 were discarded. Triangle sides were distributed into 16 length bins, each 1 Å wide, covering lengths
399 from 0 to 16 Å. A combination of three sorted side lengths, each belonging to one of 16 distance bins,
400 defines one of 508 categories of the triangles. The number of triangles of each category was calculated,
401 resulting in a 508-dimensional vector which is used as a numerical descriptor of the binding pocket
402 shape. For further operations with descriptors, Euclidian metric was introduced. Shape descriptors were
403 distributed into 6 clusters using k-means algorithm (Jain 1988). For each cluster, a centroid structure
404 was defined as the one, whose descriptor is the closest to mean descriptor for the cluster. The centroid
405 structures (2O2T#B.pdb, 1VA8#3.pdb, 2DLU#01.pdb, 1UHP#8.pdb, 2OS6#8.pdb, 3LNX#A.pdb) were
406 used for docking.

407

408 **PDZ targeted library design**

409 Screening collection by Enamine Ltd. (Chuprina 2010) containing a total of 1,195,395 drug-like
410 compounds was used as the primary source of small molecules. Natural ligand of PDZ is the C-terminus
411 of a peptide with carboxylic group making extensive hydrogen bond network with the “ΦGΦ” motif.

412 Since the carboxyl provides either of negative charge and hydrogen bond acceptor, we want our ligands
413 to retain at least one of these features. Therefore, we pre-filtered the stock library to bear chemical
414 groups which have negatively charged and/or hydrogen bond acceptor functionality. In total 65,288
415 compounds were selected for the virtual screening study. The selected 6 centroids of PDZ domains and
416 the prepared compound set were subjected to high-throughput docking using the QXP/Flo software
417 (McMartin 1997). Complexes were generated with 100 steps of sdock + routine, and 10 conformations
418 per complex were saved.

419 Processing of docking poses started with filtering by contact term *Cntc* from the QXP/Flo scoring
420 function. Entries with *Cntc* < 45 were discarded, which removed complexes with weak geometries of
421 bound ligands. The remained filtering was performed with the in-house MultiFilter program that allows
422 flexible geometry-based filtering. We applied two algorithms, *nearest-atom* filter and *hydrogen-bond*
423 filter. The former filters complexes by distance from a given protein atom to the nearest heavy ligand
424 atom, while in the latter, filtering is based upon the number of hydrogen bonds calculated for a given
425 complex geometry. With the *nearest-atom* routine we selected compounds that filled the P₀ pocket and
426 sterically mimicked binding of a peptide carboxylic group. Peptide group hydrogens of the “ΦGΦ” motif
427 and atoms forming the hydrophobic pocket were used for that. With the *hydrogen-bond* filter we selected
428 compounds that formed extensive hydrogen bonding with the PDZ domain. Both these properties might
429 have larger impact on binding rather than negative charge (Harris 2003). Details on atoms used for
430 filtering and thresholds for *hydrogen-bond* filtering, as well as the resulting number of compounds, are
431 provided in Supporting Information Table S5. Compounds from complexes which passed through these
432 filters were incorporated into a targeted library for the PDZ-domain family. The final library contained
433 1119 compounds in total.

434

435 **Screening of compounds**

436 Two-dimensional ¹H-¹⁵N HSQC spectra were used to screen a library of 212 compounds designed by
437 the company Enamine for PDZ domains. 50 μM of ¹⁵N-labeled protein samples were prepared in a 20
438 mM sodium phosphate buffer, containing 50 mM sodium chloride, 0.02% (w/v) NaN₃, at pH 7.4. Stock
439 solutions of small molecules were prepared in DMSO-*d*₆ at a concentration of 160 mM. A ¹H-¹⁵N HSQC

440 spectrum of Dvl PDZ was acquired at 300 K with 5% DMSO-*d*₆ in the absence of ligand as reference
441 spectrum. Mixtures of 16 compounds were added to ¹⁵N-labeled Dvl PDZ at 8-fold molar excess each.
442 The final concentration of DMSO-*d*₆ in the protein-ligand solutions was 5%. Spectra were acquired
443 with 8 scans and 256 points in the indirect dimension. Compound binding was deduced if the resonance
444 position of a cross-peak was significantly shifted compared to the reference spectrum. The active
445 compound was obtained through successive deconvolution. Experiments were recorded on a Bruker
446 DRX600 spectrometer equipped with a triple-resonance cryoprobe. The preparation of samples was
447 done automatically by a Tecan Genesis RSP 150 pipetting robot. Spectra were analysed using the
448 programs TOPSPIN and SPARKY.⁴⁷

449

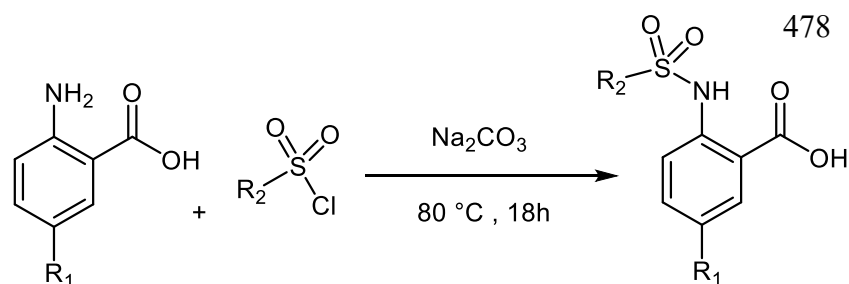
450 **Synthesis of compounds**

451 All reagents and starting materials were purchased from Sigma-Aldrich Chemie GmbH, ABCR GmbH
452 & Co.KG, alfa Aesar GmbH & Co.KG or Acros Organics and used without further purification. All air
453 or moisture-sensitive reactions were carried out under dry nitrogen using standard Schlenk techniques.
454 Solvents were removed by evaporation on a Heidolph Laborota 4000 with vacuum provided by a PC
455 3001 Vaccubrand pump. Thin-layer chromatography (TLC) was performed on plastic-backed plates pre-
456 coated with silica gel 60 F₂₅₄ (0.2 mm). Visualization was achieved under an ultraviolet (UV) lamp (254
457 and 366 nm). Flash chromatography was performed using J.T Baker silica gel 60 (30-63 μm). Analytical
458 high-performance liquid chromatography (HPLC) was performed on a Shimadzu LC-20 (degasser
459 DGU-20A3, controller CBM-20A, autosampler SIL-20A) with a DAD-UV detector (SPD-M20A),
460 using a reverse-phase C18 column (Nucleodur 100-5, 5 μM, 250 mm x 4 mm, Macherey-Nagel, Düren,
461 Germany). Separation of compounds by preparative HPLC was performed on a Shimadzu LC-8A
462 system equipped with a UV detector (SPD-M20A), using a semi-preparative C18 column (Nucleodur
463 100-5, 5 μM, 250 mm x 10 mm, Macherey-Nagel) or preparative C18 column (Nucleodur 100-5, 5 μM,
464 250 mm x 21 mm, Macherey-Nagel). The detection wavelength was 254 nm. Gradients of acetonitrile-
465 water with 0.1% TFA were used for elution at flow rates of 1 mL/min, 8 mL/min, and 14 mL/min on
466 the analytical, semi-preparative and preparative columns respectively. Melting points (mp) were
467 determined with Stuart Melting Point Apparatus SMP3 and are not corrected. Mass spectra were

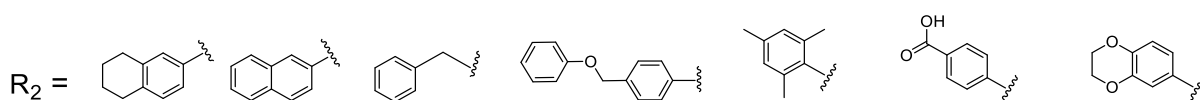
468 recorded on a 4000Q TRAP LC/MS/MS/ System for AB Applied Biosystems MDS SCIEX. NMR
469 spectra were recorded on a Bruker AV300 spectrometer instrument operating at 300 MHz for proton
470 frequency using DMSO-*d*6 solutions. Chemical shifts were quoted relative to the residual DMSO peak
471 (¹H: δ = 2.50 ppm, ¹³C: δ = 39.52 ppm). Coupling constants (J) are given in Hertz (Hz). Splitting patterns
472 are indicated as follows: singlet (s), doublet (d), triplet (t), quartet (q), multiple (m), broad (b). Purity of
473 each compound used for biological testing was ≥95% unless otherwise noted. The purity check of known
474 inhibitors purchased for comparison with our compounds are found in Supporting Information Figure
475 S9.

476

477 Synthesis of compounds 8, 11 – 17



R₁ = CF₃, Br, Cl



480 **Scheme 3:** Synthesis of compounds 8, 11 - 17

481 To a solution of anthranilic acid substituted with the appropriate R₁ (1.32 mmol) and sodium carbonate
482 (3.17 mmol) in water (2 mL) at 80 °C, the sulfonyl chloride (1.58 mmol) substituted with the appropriate
483 R₂ was added over a period of 5 minutes. The stirring continued for 18 h at 80 °C. The reaction mixture
484 was cooled to room temperature and acidified with 6 N HCl, and the resulting solid precipitate was
485 filtered, washed with water and dried to give the crude product. The final product was obtained by
486 preparative HPLC (Puranik 2008).

487

488 **2-(5,6,7,8-tetrahydronaphthalene-2-sulfonamido)- 5- (trifluoromethyl) benzoic acid (8)**

489 (0.52 g, 74% yield) ¹H-NMR (300 MHz, DMSO-d₆): δ = 11.77 [s, 1H, COOH], 8.13 [s, 1H, NH],
490 7.85 [d, ³J_{6,4} = 2.1 Hz, 1H, 6-H_{Ar}] 7.62 [d, ⁴J_{1',3'} = 2.1Hz, 1H, 1'-H_{Ar}] 7.53 [dd, ³J_{4,3} = 7.1 Hz, ⁴J_{4,6} =
491 2.1 Hz, 4-H_{Ar}] 7.36 [dd, ³J_{3',4'} = 7.5 Hz, ⁴J_{3',1'} = 2.4 Hz, 1H, 3'-H_{Ar}] 7.15 [d, ³J_{4',3'} = 7.5Hz, 1H,4'-H_{Ar}]
492 , 6.90 [d, ³J_{3,4} = 7.1Hz, 1H, 3-H_{Ar}] 2.73 (m, 4H, CH₂); 1.6 (m, 4H, CH₂); ¹³C-NMR (75 MHz, DMSO-
493 d₆): δ = 169.1(C, C_{Ar}-8), 152.7(C, C_{Ar}-2), 143.8 (C, C_{Ar}-4a'), 138.7(C, C_{Ar}-2'), 135.9 (C, C_{Ar}-8a'),
494 130.4(CH, C_{Ar}-4), 128.7 (CH, C_{Ar}-6), 127.5 (CH, C_{Ar}-1'), 124.0 (CH, C_{Ar}-4'), 121.6 (C, C-6), 118.2 (C,
495 C_{Ar}-5), 116.9 (C, C_{Ar}-3), 29.0 (CH₂, C-8'), 28.8 (CH₂, C-5'), 22.3 (CH₂, C-6'), 22.2 (CH₂, C-7'); mp:
496 177°C; MS (ESI) *m/z*: calcd. for C₁₈H₁₆F₃NO₄S, 399; found 400 [M+H]⁺.

497 **5-bromo-2-(naphthalene-2-sulfonamido) benzoic acid (11)**

498 (0.13 g, 67% yield) ¹H-NMR (300 MHz, DMSO-d₆): δ = 10.2 [s, 1H, COOH], 9.8 [s, 1H, NH] 8.59 [d,
499 ⁴J_{1',3'} = 1.4 Hz, 1 H, 1'-H_{Ar}], 8.17 [d, ³J_{8',7'} = 7.8 Hz, 1 H, 8'-H_{Ar}], 8.10 [d, ³J_{4',3'} = 8.8 Hz, 1 H, 4'-H_{Ar}],
500 8.02 [d, ³J_{5',6'} = 7.8 Hz, 1 H, 5'-H_{Ar}], 7.93 [d, ⁴J_{6,4} = 2.4 Hz, 1 H, 6-H_{Ar}], 7.77 [dd, ³J_{3',4'} = 8.8 Hz, ⁴J_{3',1'}
501 = 1.4Hz, 1 H, 3'-H_{Ar}], 7.72 – 7.65 [m, 3 H, 4-H_{Ar}, 6'-H_{Ar}, 7'-H_{Ar}], 7.51 [d, ³J_{3,4} = 8.9 Hz, 1 H, 3-H_{Ar}]. –
502 ¹³C-NMR (75 MHz, DMSO-d₆): δ = 168.2 (C, C-7), 138.8 (C, C_{Ar}-2), 136.8 (CH, C_{Ar}-4), 135.3 (C, C_{Ar}-
503 4a'), 134.4 (C, C_{Ar}-8a'), 133.4 (CH, C_{Ar}-6), 131.4 (CH, C_{Ar}-6'), 129.3 (CH, C_{Ar}-4'), 128.5 (CH, C_{Ar}-
504 8'), 127.8 (2xCH, C_{Ar}-5', C_{Ar}-7') 121.6 (CH, C_{Ar}-3'), 120.6 (CH, C_{Ar}-3), 119.0 (C, C_{Ar}-1), 114.9 (C, C_{Ar}-
505 5). Mp: 199°C; (ESI) *m/z*: calcd. for C₁₇H₁₁BrNO₄S⁻; 403.9560; found 403.9613 [M-H]⁻.

506 **5-bromo-2-(phenylmethylsulfonamido)benzoic acid (12)**

507 (0.07g, 42% yield) ¹H-NMR (300 MHz, DMSO-d₆): δ = 10.57 [s, 1 H, COOH], 8.05 [d, ⁴J_{6,4} = 2.4
508 Hz, 1 H, 6-H_{Ar}], 7.75 [dd, ³J_{4,3} = 8.9 Hz, ⁴J_{4,6} = 2.4Hz, 1 H, H-4_{Ar}], 7.49 [d, ³J_{3,4} = 8.9 Hz, 1 H, 3-H_{Ar}],
509 7.33 – 7.28 [m, 3 H, 3'-H_{Ar}, 5'-H_{Ar}], 7.23 – 7.20 [m, 2 H, 4'-H_{Ar}], 5.75 [s, 1 H, NH], 4.72 [s, 2 H, 1'-
510 H] ¹³C-NMR (75 MHz, DMSO-d₆): δ = 168.3 (C, C-7), 139.9 (C, C_{Ar}-2), 137(CH, C_{Ar}-4), 133.4 (CH,
511 C_{Ar}-6), 130.7 (CH, C_{Ar}-3'), 128.6 (C, C_{Ar}-2'), 128.4 (CH, C_{Ar}-5'), 128.3 (CH, C_{Ar}-4'), 119.5 (CH,
512 C_{Ar}-3), 117.5 (C, C_{Ar}-1), 113.9 (C, C_{Ar}-5), 57.4 (CH₂, C-1'). Mp: 216°C; (ESI) *m/z*: calcd. for
513 C₁₄H₁₁BrNO₄S⁻ 367.9860; found 367.9878 [M-H]⁻.

514 **5-bromo-2-(4-(phenoxy)methyl)phenylsulfonamido)benzoic acid (13)**

515 (0.6 g, 29% yield) ¹H-NMR (300 MHz, DMSO-d₆): δ = 7.97 [d, ⁴J_{6,4} = 2.4 Hz, 1 H, 6-H_{Ar}], 7.85 (d,
516 ³J_{2',3'} = 8.3 Hz, 2 H, 3'-H_{Ar}), 7.73 [dd, ³J_{4,3} = 8.9 Hz, ⁴J_{4,6} = 2.4Hz, 1 H,4-H_{Ar}], 7.63 [d, ³J_{2',3'} = 8.3 Hz, 2

517 H, 2'-H_{Ar}], 7.47 [d, ³J_{3,4} = 8.9 Hz, 1 H, 3-H_{Ar}], 7.29 [dd, ³J_{3',2''} = ³J_{3',4''} = 7.3 Hz, 2 H, 3''-H_{Ar}], 7.00 – 6.92
518 [m, 3 H, 4''-H_{Ar}, 2''-H_{Ar}], 5.17 [s, H, 5'-H]. – **¹³C-NMR** (75 MHz, DMSO-d₆): δ = 168.2 (C, C-7),
519 157.9 (C, C_{Ar}-1''), 143.2 (C, C_{Ar}-4'), 138.8 (C, C_{Ar}-2), 137.5 (C, C_{Ar}-1'), 136.9 (CH, C_{Ar}-4) 133.5 (CH,
520 C_{Ar}-6), 129.4(CH, C_{Ar}-3''), 128.1(CH, C_{Ar}-2'), 127.0 (CH, C_{Ar}-3'), 120.9 (CH, C_{Ar}-4''), 120.5 (CH, C_{Ar}-
521 3), 119.0 (C, C_{Ar}-1), 114.9(CH, C_{Ar}-5), 114.7 (CH, C_{Ar}-2''), 68.0 (CH₂, C-5') Mp: 175°C; (ESI) m/z:
522 calcd for C₂₀H₁₅BrNO₅S- 459.9860 found 459.9878 [M-H].

523 **5-bromo-2-(2,4,6-trimethylphenylsulfoamido)benzoic acid (14)**

524 (0.6 g, 78% yield) **¹H-NMR** (300 MHz, DMSO-d₆): δ = 11.77 [s, 1H, COOH], 9.98 [s, 1H, NH], 7.68
525 [d, ³J_{6,4} = 7.4 Hz, 1H, 6-H_{Ar}], 7.51 [dd, ³J_{4,3} = 7.1 Hz, ⁴J_{4,6} = 7.4 Hz, 1H 4-H_{Ar}], 7.17 [d, 2H, 4'-H_{Ar}, 6'-
526 H_{Ar}], 7.14 [d, ³J_{3,4} = 1H, 3-H_{Ar}], 2.56 [s, 6H, CH₃, 9'-H, 7'-H], 2.21 [s, 3H, CH₃, 8'-H]; -**¹³C-NMR** (300
527 MHz, DMSO-d₆): δ = 168.8 (C, C-7), 143.3 (C, C_{Ar}-2), 139.5 (C, C_{Ar}-2'), 139.0 and 139.0 (2x C, C_{Ar}-
528 3', C_{Ar}-1') 137.3 (CH, C_{Ar}-4), 134.0 (CH, C_{Ar}-6'), 133.0 (CH, C_{Ar}-6), 132.5 and 132.5 (2XCH, C_{Ar}-4',
529 C_{Ar}-6') 119.1(CH, C_{Ar}-3), 117.9(C, C_{Ar}-5), 114.3 (C, C_{Ar}-1), 22.5 and 22.5 (2 x CH₃, C-7', C-9') 20.7
530 (CH₃, C-8'); mp: 185; MS (ESI): m/z 399 [M+H]⁺.
531

532 **2-(4-acetylphenylsulfoamido)-5-(trifluoromethyl)benzoic acid (15)**

533 (0.4 g, 63% yield) **¹H-NMR** (300 MHz, DMSO-d₆): δ = 12.28 [s, 1H, COOH]; 12.10 [s, 1H, NH], 8.11
534 [d, ⁴J_{6,4} = 2.5 Hz, 1H, 6-H_{Ar}], 8.08 [d, ³J_{3',2'} = 7.5 Hz, 2H, 3'-H_{Ar}], 7.86 [dd, ⁴J_{4,6} = 2.5 Hz, ³J_{4,3} = 7.3 Hz,
535 1H, 4-H_{Ar}], 7.64 [d, ³J_{4,3} = 7.3 Hz, 1H, 3-H_{Ar}], 7.56 [dd ³J_{2',3'} = 7.5 Hz, ⁴J_{2',6'} = 2.3 Hz, 2H, 2'-H_{Ar}, 6'-
536 H_{Ar}] 7.22 [dd, ³J_{3',2'} = 7.5 Hz, ⁴J_{3',5'} = 2.1 Hz, 2H, 3'-H_{Ar}, 5'-H_{Ar}] 2.50 [s, 3H, CH₃, 8'-H]; - **¹³C-NMR**
537 (75 MHz, DMSO-d₆): δ = 197.9 (C, C-7'), 169.1(C, C-8), 151.8 (C, C_{Ar}-2) 143.5 (C, C_{Ar}-1'), 142.5 (C,
538 C_{Ar}-4'), 140.6 (CH, C_{Ar}-4), 131.4 (CH, C_{Ar}-7), 129.6 (2XCH, C_{Ar}-3', C_{Ar}-5'), 128.6 (2XCH, C_{Ar}-2', C_{Ar}-
539 6'), 127.6 (C, C_{Ar}-6), 123.0 (C, C_{Ar}-5), 118.7 (CH, C_{Ar}-3), 27.3 (CH₃, C-8'); mp: 170°C; MS (ESI) m/z
540 : calcd. for C₁₆H₁₂F₃NO₅S. 387; found 388 [M+H]⁺.

541 **2-(2,3-dihydrobenzo[b][1,4]dioxine-6-sulfonamido)-5-(trifluoromethyl)benzoic acid (16)**

542 (0.4 g, 65% yield) **¹H-NMR** (300 MHz, DMSO-d₆): δ = 11.48 [s, 1H, COOH], 8.13 [s, 1H, NH], 7.89
543 [d, ⁴J_{6,4} = 3.9 Hz, 1H, 6-H_{Ar}] 7.66 [dd, ³J_{4,3} = 7.2 Hz, ⁴J_{4,6} = 4.3 Hz, 1H, 4-H_{Ar}],
544 7.23 [d, ³J_{4,3} = 7.2 Hz 1H, 3-H_{Ar}], 7.11 [dd, ³J_{2',3'} = 7.3 Hz, ⁴J_{2',8'} = 3.2 Hz, 1H, 2'-H_{Ar}] 6.95 [d, ⁴J_{2',8'} =
545 3.2 Hz, 1H, 8'-H_{Ar}] 4.23 – 4.31 [m, 4H, 5'-H, 6'-H]; - **¹³C-NMR** (75-MHz, DMSO-d₆): δ = 168.9(C,

546 C-8), 148.3 (C, C-4'), 143.8 (C, C-2), 143.5 (C, C-7'), 131.3 (C, C-1'), 130.8 (CH, C-4), 128.6 (CH, C-
547 6), 125.7 (C, C-7), 122.1 (C, C-5), 120.9 (CH, C-2'), 118.3 (CH, C-3), 118.1 (CH, C-3'), 116.8 (CH, C-
548 8'), 64.7 (CH₂, C-5') 64.3 (CH₂, C-6'); mp: 178°C; MS (ESI) *m/z*: calcd. for C₁₆H₁₂F₃NO₆S. 403; found
549 404 [M+H]⁺.

550 **5-(trifluoromethyl)-2-(2,4,6-trimethylphenylsulfoamido)benzoic acid (17)**

551 (0.38 g, 62% yield) ¹H-NMR (300 MHz, DMSO-*d*₆): δ = 12.28 [s, 1H, COOH], 11.60 [s, 1H, NH], 8.15
552 [d, ⁴J_{6,4} = 4.3 Hz, 1H, 6-H_{Ar}] 7.92 [dd, ³J_{4,3} = 7.9 Hz, ⁴J_{4,6} = 2.1 Hz, 1H, 4-H_{Ar}] 7.87 [d, ⁴J_{6',4'} = 1.9 Hz, 2H,
553 4'-H_{Ar}, 6'-H_{Ar}], 7.48 [d, ³J_{3,4} = 7.9 Hz, 1H, 3-H_{Ar}], 2.60 [s, 6H, CH₃, 9'-H, 7'-H], 2.23 [s, 3H, CH₃,
554 8'-H]; - ¹³C-NMR (75 MHz, DMSO-*d*₆): δ = 169.3 (C, C-7), 154.2 (C, C-2), 143.6 (C, C-2'), 139.1
555 and 139.1 (2xC, C-1', C-3') 132.9 (C, C-5'), 132.5 (CH, C-4), 131.5 and 131.5 (2xCH, C-4', C-6'),
556 130.1 (CH, C-6), 128.7 (C, C-8), 122.5 (C, C-5), 117.0 (CH, C-3), 109.0 (C, C-1), 22.4 and 22.4
557 (2xCH₃, C-7', C-9'), 20.8 (CH₃, C-8'); mp: 184°C; MS (ESI) *m/z*: calcd. for C₁₇H₁₆F₃NO₄S; 387; found
558 388 [M+H]⁺.

559

560 **18, 19, 20, and 21** were purchased from Enamine, Kiev, Ukraine as pure compounds (see also Table S6,
561 Supporting Information).

562

563 **Determination of ligand binding and binding constant by NMR**

564 50 μM of ¹⁵N-labeled protein samples were prepared in a 20 mM sodium phosphate buffer containing
565 50 mM sodium chloride, 0.02 % (w/v) NaN₃, at pH 7.4. Stock solutions of small molecules were
566 prepared in DMSO-*d*₆ at a concentration of 160 mM. A ¹H-¹⁵N HSQC spectrum of Dvl PDZ was
567 acquired at 300 K with 5% DMSO-*d*₆ in the absence of ligand as reference spectrum. Mixtures of 16
568 compounds were added to ¹⁵N-labeled Dvl PDZ at 8-fold molar excess each. The final concentration of
569 DMSO-*d*₆ in the protein-ligand solutions was 5%. Spectra were acquired with 8 scans and 256 points
570 in the indirect dimension.

571 Binding was deduced if the resonance position of a cross-peak was significantly shifted compared to the
572 reference spectrum. The active compound was obtained through successive deconvolution. Experiments
573 were recorded on a Bruker DRX600 spectrometer equipped with a triple-resonance cryoprobe. The

574 preparation of samples was done automatically by a Tecan Genesis RSP 150 pipetting robot. Spectra
575 were analysed using the programs TOPSPIN and SPARKY.

576 Chemical shift perturbations were obtained by comparing the ^1H - ^{15}N backbone resonances of protein
577 alone to those of protein-ligand complex. The mean shift difference ($\Delta\delta$ in ppm) was calculated using
578 the equation 1 (Garrett 1997, Bertini 2011).

$$579 \quad \Delta\delta = \sqrt{\frac{[\Delta\delta_H]^2 + [\Delta\delta_N/5]^2}{2}} \quad (\text{Eq. 1})$$

580 Here $\Delta\delta_N$ and $\Delta\delta_H$ are the amide nitrogen and amide proton chemical shift differences between the free
581 and the bound states of the protein. In order to estimate binding constants, titration experiments
582 monitored by NMR were done. A series of ^1H - ^{15}N HSQC were recorded as a function of ligand
583 concentration. Residues showing a continuous chemical shift change and for which the intensity
584 remained strong were classified as being in fast exchange. The dissociation binding constant was
585 estimated by fitting the observed chemical shift change to equation 2 (Shuker 1996, Hajduk 1997).

$$586 \quad \frac{\Delta\delta}{\Delta\delta_{max}} \\ 587 \quad = \frac{([L_T] + [P_T] + K_D) - \sqrt{([L_T] + [P_T] + K_D)^2 - 4[L_T] \cdot [P_T]}}{2[P_T]} \quad (\text{Eq. 2})$$

588
589 $\Delta\delta$ is the observed protein amide chemical shift change at a given compound concentration and $\Delta\delta_{max}$
590 the maximum chemical shift change at saturation. $[L_T]$ the total concentration of the compound, and $[P_T]$
591 the total concentration of the protein. K_D is the equilibrium dissociation constant. The K_D values are
592 reported as means \pm standard deviations of at least six residues influenced upon binding of the ligand.

593

594 **Determination of binding constant by Isothermal Titration Calorimetry (ITC)**

595 Isothermal Titration Calorimetry (ITC) experiments were performed using a VP-ITC system
596 (MicroCal). Protein in 20 mM Hepes buffer, 50 mM NaCl, pH 7.4, was centrifuged and degassed before
597 the experiment. A 200 μM ligand solution containing 2% DMSO was injected 30 times in 10 μL aliquots
598 at 120 s intervals with a stirring speed of 1000 rpm into a 1.4 mL sample cell containing the Dvl PDZ

599 domain at a concentration of 20 μ M at 25 °C. Control experiment was initially determined by titrating
600 ligand into buffer at same conditions. Titration of ligand into buffer yielded negligible heats.
601 Thermodynamic properties and binding constants were determined by fitting the data with a nonlinear
602 least-squares routine using a single-site binding model with Origin for ITC v.7.2 (Microcal).

603

604 **Protein expression**

605 PDZ domains of human AF6 (P55196-2, residues 985–1086) and murine α 1-syntrophin (Q61234,
606 residues 81–164) were cloned into pGEX-6P-2 (Amersham Biosciences, Freiburg, Germany) and
607 pGAT2 (European Molecular Biology Laboratory, Heidelberg, Germany), respectively. Proteins were
608 expressed in *E. coli* BL21 (DE3) cells and purified as previously described (Boisguerin 2004). For the
609 cloning of the Dvl-1 PDZ domain (O14640, residues 245–338), IMAGp958J151157Q (ImaGenes) was
610 used as template. V250 is exchanged to isoleucine as in human Dvl-3 or murine Dvl-1. The C-terminal
611 C338 of the domain was exchanged by serine. Via cloning in pET46EK/LIC, a coding sequence for a
612 TEV (Tobacco Etch Virus) protease cleavage site was introduced. The resulting plasmid pDVL1 was
613 transformed in *E. coli* BL21 (DE3). Expression on two-fold M9 minimal medium with 0.5 g/L 15 N
614 NH_4Cl as sole nitrogen source in shaking culture was done at 25 °C overnight with 1 mM IPTG. A yield
615 of 25 mg of pure Dvl-1 was obtained from 1 L culture after IMAC, TEV protease cleavage, a second
616 IMAC, and gel filtration (Superdex 75). The protein domain Dvl-1_245–338 was supplied for NMR in
617 20 mM phosphate buffer, pH 7.4, 50 mM NaCl.

618 The production of Dvl-3 (Q92997 residues 243-336), mShank3 (Q4ACU6, residues 637-744) PDZ
619 domains and the 3 PDZ domains of PSD95 was described by Saupe et al (Saupe 2011).

620

621 **Crystallization and X-ray diffraction**

622 The His-tagged cleaved human Dvl-3 PDZ domain was concentrated to 12-20 mg/mL in the presence
623 of a 5-fold molar excess of compound **3**, **5**, **6**, **7**, **11** and **12**. Crystals of all complexes were grown at
624 room temperature by the sitting drop vapour-diffusion method. 200 nL Dvl-3/compound solution was
625 mixed with an equal volume of reservoir solution using the Gryphon (Formulatrix) pipetting robot.
626 Crystals of all complexes were grown to their final size within 4 to 14 days. The Dvl-3 PDZ domain

627 crystallized in complex with compound **3** and **7** in crystallization condition 30% PEG 8000, 0.2 M
628 ammonium sulphate, 0.1 M MES pH 6.5; with compound **5** in 30% PEG 8000, 0.1 M MES pH 5.5; with
629 compound **6** in 1.2 M ammonium sulphate, 0.1 M citric acid pH 5.0; with compound **12** in 32% PEG
630 8000, 0.2 M ammonium sulphate, 0.1 M Na-cacodylate pH 6.0; with compound **11** in 1 M ammonium
631 sulphate, 1% PEG 3350, 0.1 M Bis-Tris pH 5.5; with compound **12** in 1.26 M sodium phosphate, 0.14
632 M potassium phosphate and with compound **18** in 1.5 M ammonium sulphate, 12% glycerol, 0.1 M Tris-
633 HCl pH 8.5. The crystals were cryoprotected if necessary, for data collection by soaking for few seconds
634 in precipitant solution containing 20% (v/v) glycerol and subsequently frozen in liquid nitrogen.
635 Diffraction data were collected at 100 K at beamline BL14.1 at the synchrotron-radiation source BESSY,
636 Helmholtz-Zentrum Berlin and processed with XDS.

637

638 **Structure determination and refinement**

639 Phases for the Dvl-3 PDZ domain in complex with compound **3** were obtained by molecular replacement
640 with PHASER (McCoy 2007) using the *Xenopus laevis* Dishevelled PDZ domain structure (PDB code
641 2F0A) as a starting model. The reasonable crystal packing and electron density allowed further model
642 and compound building using the program COOT (Emsley 2004) with iterative refinement with
643 REFMAC (Murshudov 1997). All further complex structures were obtained in the same way but using
644 the final refined compound free Dvl-3-PDZ structure as model for molecular replacement. The
645 Ramachandran statistics were analysed by Molprobity (Chen 2010) for all complexes and all
646 crystallographic statistics are given in Supporting Information Tables S2 and S3. Figures were prepared
647 with PyMol. Atomic coordinates and structure factor amplitudes for DVL-3 PDZ domain in complex
648 with compound **3**, **5**, **6**, **7**, **11**, **12**, **18** were deposited in the Protein Data Bank with accession codes
649 6ZBQ, 6ZBZ, 6ZC3, 6ZC4, 6ZC6, 6ZC7 and 6ZC8, respectively.

650

651 **MTT assay**

652 HEK293 cells were plated on a 96-well plate and treated with different concentrations of Dvl inhibitors.
653 After 24 h treatment, 20 μ l of MTT solution (5 mg/mL) was added into each well. After 2 h incubation,

654 cell culture medium was replaced with 50 μ L DMSO, and the signal of the purple formazan, produced
655 by living cells, was measured by a plate reader.

656

657 **TOP-GFP reporter assay**

658 The lentivirus particle (CCS-018L, SABiosciences) encoding GFP under the control of a basal promoter
659 element (TATA box) joined to tandem repeats of a consensus TCF/LEF binding site was transfected
660 into HEK293 cells. Stable cells were selected by puromycin (2 μ g/mL) treatment. Wnt signalling
661 activity indicated by GFP intensity was measured by flow cytometry after 24 h incubation with
662 recombinant mouse Wnt3a (100 ng/mL) or GSK3 inhibitor CHIR99021 (3 μ M) in the presence of Dvl
663 inhibitors.

664

665 **Luciferase reporter assays**

666 Plasmids encoding a firefly luciferase reporter gene under the control of different responsive elements
667 were transfected into Hela cells with a pRL-SV40 normalization reporter plasmid using the
668 Lipofectamine 2000 (Invitrogen). After desired treatment, cells were harvested in the passive lysis buffer
669 (Promega), and 15 μ L cell lysate were transferred to 96-well LumiNunc plates (Thermo Scientific).
670 Firefly luciferase and Renilla luciferase were detected with the D-luciferin buffer (75 mM Hepes, 4 mM
671 MgSO₄, 20 mM DTT, 100 μ M EDTA, 0.5 mM ATP, 135 μ M Coenzyme A and 100 μ M D-Luciferin
672 sodium salt, pH 8.0) and the coelenterazine buffer (15 mM Na₄PPi, 7.5 mM NaAc, 10 mM CDTA, 400
673 mM Na₂SO₄, 25 μ M APMBT and 1.1 μ M coelenterazine, pH 5.0) respectively using the CentroXS
674 LB960 lumimeter (Berthold Technologies).

675

676 **Immunoblotting**

677 To assess the β -catenin accumulation in Hela cells, cells were treated with Wnt3a in the presence of Dvl
678 inhibitors for 24 h and lysed in RIPA buffer (50 mM Tris, pH 8.0, 1% NP-40, 0.5% deoxycholate, 0.1%
679 SDS, 150 mM NaCl). Equal amounts of protein were loaded on a SDS-PAGE. Separated proteins were
680 blotted onto PVDF membranes for immunoblot analysis using anti- β -catenin antibody (610154, BD).
681 HRP-conjugated anti-mouse antibody (715-035-150, Jackson ImmunoResearch laboratories) was used

682 for secondary detection with Western lightning chemiluminescence reagent plus (PerkinElmer) and
683 Vilber Lourmat imaging system SL-3.

684

685 **qRT-PCR analysis**

686 To measure the Wnt target accumulation at mRNA level, Hela cells were treated with Wnt3a in the
687 presence of Dvl inhibitors for 24 h. mRNA was extracted according to the standard TRIzol® protocol
688 (Invitrogen) and reverse-transcribed using random primers (Invitrogen) and M-MLV reverse
689 transcriptase (Promega). The qRT-PCR was performed in iQ5 Multicolor Real-Time PCR Detection
690 System (Bio-Rad) using SYBR® Green (Thermo Scientific) and gene-specific primer pairs of Bmp2,
691 Axin2, Lef1 and β -actin (endogenous control).

692

693 **Migration assay**

694 Cell motility was assessed using 24-well transwell (pore diameter: 8 μ m, Corning). SW480WL cells
695 were seeded in the upper chamber in serum free DMEM with 0.1% BSA; 20% serum was supplemented
696 to medium in the lower chamber. After incubation with Wnt3a in the presence of Dvl inhibitors for 24
697 h, nonmigrant cells were scraped off using a cotton swab; the migrated cells on the filters were stained
698 with DAPI, photographed and counted.

699

700 **Colon sphere culture**

701 SW480WL cells were trypsinised into single cells, seeded on 24-well cell culture plates precoated with
702 250 μ l polyhema (12 mg/mL in 95% ethanol, Sigma) per well, and incubated with Wnt3a in the presence
703 of Dvl inhibitors in the sphere culture medium (F12 : DMEM 1 : 1, 1X B-27 supplement, 20 ng/mL
704 EGF, 20 ng/mL FGF, 0.5% methylcellulose) for 10 days. Numbers of spheres were then counted under
705 the microscope.

706

707 **Notes**

708 The authors declare no competing financial interest.

709

710 **ACKNOWLEDGEMENTS**

711 This research was supported by the Deutsche Forschungsgemeinschaft (DFG) Research Group 806 and
712 the EU-project iNext (Infrastructure for NMR, EM and X-rays for Translational Research, GA 653706).
713 We thank M. Leidert and S. Radetzki for protein preparation, and B. Schlegel for NMR assistance. We
714 also thank E. Specker for compound analysis.

715 **ABBREVIATIONS USED**

716 NMR, nuclear magnetic resonance; HSQC, Heteronuclear Single Quantum Correlation;
717 AU, asymmetric unit; SAR, derive structure activity relationships; vdW, van der Waals;
718 ITC, Isothermal titration calorimetry; PDZ, PSD95/Disc large/Zonula occludens 1);
719 Dvl, Dishevelled; PPI, protein-protein interactions; PDB, Protein Data Bank;
720 CSP, chemical shift perturbation; GFP, green fluorescent protein; DMSO, dimethyl sulfoxide;
721 PEG, polyethylene glycol; RNA, ribonucleic acid; mRNA, messenger RNA;
722 qRT-PCR, quantitative real-time polymerase chain reaction; DMEM Dulbecco's modified Eagle's
723 medium ; BSA, bovine serum albumin;

724

725 **ASSOCIATED CONTENT**

726

727 **Accession Codes**

728 Atomic coordinates and structure factor amplitudes for DVL3 PDZ domain in complex with compound
729 **3, 5, 6, 7, 11, 12, 18** were deposited in the Protein Data Bank with accession codes 6ZBQ, 6ZBZ, 6ZC3,
730 6ZC4, 6ZC6, 6ZC7 and 6ZC8, respectively. Authors will release the atomic coordinates and
731 experimental data upon article publication.

732

733 **Supporting information**

734 **1.** Structure-based alignment of the amino acid sequences of Dvl-1,2,3 PDZ ; PSD95-PDZ-1,2,3 ; Af-
735 6 and Syn PDZ domains. (S.2)

736 **2.** 1H-15N HSQC spectra of Dvl-3 PDZ domain alone and in the presence of varying concentrations of
737 compound 3. (S.3)

- 738 3. Detailed views of diverse compounds bound to the Dvl-3 PDZ domain. (S.4)
- 739 4. Cell viability assays of compounds 3, 7,8, 9, 10, (A) and 18, 20, 21 (B). (S.5)
- 740 5. ITC binding assays of compound 18 with Dvl-3 PDZ (A) and with Dvl-1 PDZ (B). (S.5)
- 741 6. Structures of selected compounds used for comparison to our compounds. (S.6)
- 742 7. ITC data of selected compounds used for comparison to our compounds. (S.7)
- 743 8. NMR binding assay with compound 322338/3289-8625. (S.8)
- 744 9. Purity check of compounds. (S.9)
- 745 – Purity check of NPL-1011 compound. (S.9)
- 746 – Purity check of Sulindac compound. (S.10)
- 747 – Purity check of CalBioChem-322338 compound. (S.11)
- 748 – Purity check of NSC668036 compound. (S.12)
- 749 – LCMS of intermediate compound 8. (S.13)
- 750 – LCMS of intermediate compound 14. (S.13)
- 751 10. Chemical shift perturbation values of Dvl-3 PDZ and Dvl-1 PDZ for compounds (3-21). (S.14)
- 752 11. Data collection and refinement statistics of compounds 3, 5, 6, 7. (S.15)
- 753 12. Data collection and refinement statistics of compounds 11, 12, 18. (S.16)
- 754 13. Selectivity of ligands derived from chemical shift perturbation of compounds tested at other PDZ
- 755 domains. (S.17)
- 756 14. Details of Multifilter routines. (S.17)
- 757 15. Smiles codes and Compounds ID. (S.18)
- 758 16. NMR characterization of synthesized compounds (8, 11, 13, 14, 15, 16, 17). (S.21)
- 759

760 **References**

- 761 Behrens, J., von Kries, J. P., Kühl, M., Bruhn, L., Wedlich, D., Grosschedl, R. and Birchmeier, W.:
762 Functional interaction of beta-catenin with the transcription factor LEF-1. *Nature*, 382, 638-642,
763 DOI: 10.1038/382638a0, 1996.
- 764 Bertini, I., Chevanace, S., Del Conte, R., Lalli, D. and Turano, P.: The anti-apoptotic Bcl-x(L) protein,
765 a new piece in the puzzle of cytochrome c interactome. *PLoS One*, 6:e18329, DOI:
766 10.1371/journal.pone.0018329, 2001.
- 767 Berman, H. M., Westbrook, J., Feng, Z., Gilliland, G., Bhat, T. N., Weissig, H., Shindyalov, I. N. and
768 Bourne, P.E.: The protein data bank, *Nucleic. Acids Res.*, 28, 235 – 242, DOI: 10.1093/nar/28.1.235,
769 2000.

770 Boisguerin, P., Leben, R., Ay, B., Radziwill, G., Moelling, K., Dong, L. and Volkmer-Engert, R.: An
771 improved method for the synthesis of cellulose membrane-bound peptides with free C termini is
772 useful for PDZ domain binding studies. *Chem. Biol.*, 11, 449 – 459, DOI:
773 10.1016/j.chembiol.2004.03.010, 2004.

774 Bui, T. D., Beier, D. R., Jonssen, M., Smith, K., Dorrington, S. M., Kaklamanis, L., Kearney, L.,
775 Regan, R., Sussman, D. J. and Harris, A. L.: cDNA cloning of a human dishevelled DVL-3 gene,
776 mapping to 3q27, and expression in human breast and colon carcinomas. *Biochem. Biophys. Res.*
777 *Commun.*, 239, 510 – 516, DOI: 10.1006/bbrc.1997.7500, 1997.

778 Chandanamali, P., Antonio, M. F., Robert, C., Patrick, R. and Naoaki, F.: Sequence and subtype
779 specificity in the high-affinity interaction between human frizzled and dishevelled proteins, *Protein*
780 *Sci.*, 18, 994 – 1002, DOI: 10.1002/pro.109, 2009.

781 Chen V. B., Arendall, W. B. 3rd, Headd, J. J. and Keedy, D. A., Immormino, R. M., Karpral, G. J.,
782 Murray, L. W., Richardson, J. S., Richardson, D. C.: MolProbity: all-atom structure validation for
783 macromolecular crystallography. *Acta Cryst.*, 66, 12 - 21, DOI: 10.1107/S0907444909042073, 2010.

784 Choi, J., Ma, S.; Kim, H.-Y., Yun, J.-H., Heo, J.-N., Lee, W., Choi, K.-Y. and No, K.: Identification of
785 small-molecule compounds targeting the dishevelled PDZ domain by virtual screening and binding
786 studies. *Bioorg. Med. Chem.*, 24, 3259–3266. Doi: 10.1016/j.bmc.2016.03.026, 2016.

787 Christensen, N. R., De Luca, M., Lever, M. B., Richner, M., Hansen, A. B., Noes-Holt, G., Jensen, K.
788 L., Rathje, M., Jensen, D. B., Erlendsson, S., Bartling, C. R., Ammendrup-Johnsen, I., Pedersen, S.
789 E., Schönauer, M., Nissen, K. B., Midtgaard, S. R., Teilum, K., Arleth, L., Sørensen, A. T., Bach, A.,
790 Strømgaard, K., Meehan, C. F., Vaegter, C. B., Gether, U. and Madsen, K. L.: A high-affinity,
791 bivalent PDZ domain inhibitor complexes PICK1 to alleviate neuropathic pain. *EMBO Mol. Med.*,
792 12 :e11248, Doi: 10.15252/emmm.201911248, 2020.

793 Christensen, N. R., Calyseva, J., Fernandes, E. F. A., et al.: PDZ Domains as Drug Targets. *Adv.*
794 *Ther.*, 2(7), 1800143, Doi:10.1002/adtp.201800143, 2019.

795 Chuprina, A., Lukin, O., Demoiseaux, R., Buzko, A. and Shivanyuk, A.: Drug- and lead-likeness,
796 target class, and molecular diversity analysis of 7.9 million commercially available organic
797 compounds provided by 29 suppliers. *J. Chem. Inf. Model.*, 50, 470 - 499. Doi: 10.1021/ci900464s,
798 2010.

799 Doyle, D. A., Lee, A., Lewis, J., Kim, E., Sheng, M. and MacKinnon, R.: Crystal structures of a
800 complexed and peptide-free membrane protein-binding domain: Molecular basis of peptide
801 recognition by PDZ. *Cell*, 85, 1067-1076, DOI: 10.1016/s0092-8674(00)81307-0, 1996.

802 Emsley, P. and Cowtan, K.: Coot: model-building tools for molecular graphics. *Acta Cryst.*, 60, 2126
803 – 2132 , DOI: 10.1107/S0907444904019158, 2004.

804 Fan, X., Quyang, N., Teng, H. and Yao, H.: Isolation and characterization of spheroid cells from the
805 HT29 colon cancer cell line. *Int. J. Colorect. Dis.*, 26, 1279 - 1285, DOI: 10.1007/s00384-011-1248-
806 y, 2011.

807 Fang, L., Von Kries, J. P. and Birchmeier, W.: Identification of small-molecule antagonists of the
808 TCF/ β -catenin protein complex, in 30 years of Wnt signalling. *EMBO Conference: Egmond aan Zee*,
809 *Netherlands*. p. 101, 2012.

810 Fanning, A. S. and Anderson, J. M.: Protein-protein interactions: PDZ domain networks. *Curr. Biol.*,
811 6, 1385 – 1388, DOI: 10.1016/s0960-9822(96)00737-3, 1996.

812 Fritzmann, J., Morkel, M., Besser, D., Budczies, J., Kosel, F., Brembeck, F. H., Stein, U., Fichtner, I.,
813 Schlag, P. M. and Birchmeier, W.: A colorectal cancer expression profile that includes transforming
814 growth factor beta inhibitor BAMBI predicts metastatic potential. *Gastroenterology*, 137, 165 - 175,
815 DOI: 10.1053/j.gastro.2009.03.041, 2009.

816 Fujii, N., You, L., Xu, Z., Uematsu, K., Shan, J., He, B., Mikami, I., Edmondson, L.R., Neale, G.,
817 Zheng, J., Guy, R. K. and Jablons, D. M.: An antagonist of dishevelled protein-protein interaction
818 suppresses β -catenin-dependent tumor cell growth. *Cancer Res.*, 67, 573 - 579, DOI: 10.1158/0008-
819 5472.CAN-06-2726, 2007.

820 Garrett, D. S., Seok Y. J., Peterkofsky A. and Gronenborn, A. M.: Identification by NMR of the
821 binding surface for the histidine-containing phosphocarrier protein HPr on the N-terminal domain of
822 enzyme I of the Escherichia coli phosphotransferase system. *Biochem.*, 36, 4393 – 4398, DOI:
823 10.1021/bi970221q, 1997.

824 Goddard, T. D. and Kneller, D. G.: SPARKY 3, University of California, San Francisco, 2003.

825 Grandy, D., Shan, J., Zhang, X., Rao, S., Akunuru, S., Li, H., Zhang, Y., Alpatov, I., Zhang, X., Lang,
826 R., Shi, De-Li. and Zheng, J.: Discovery and characterization of a small molecule inhibitor of the
827 PDZ domain of dishevelled. *J. Biol. Chem.*, 284, 16256–16263. DOI: 10.1074/jbc.M109.00 9647,
828 2009.

829 Hajduk, P. J., Sheppard, G., Nettesheim, D. G., Olejniczak, E. T., Shuker, S. B., Meadows, R. P.,
830 Steinman, D. H., Carrera, G. M. Jr., Marcotte, P. A., Severin, J., Walter, K., Smith, H., Gubbins, E.,
831 Simmer, R., Holzman, T. F., Morgan, D. W., Davidsen, S. K., Summers, J. B. and Fesik, S. W.:
832 Discovery of Potent Nonpeptide Inhibitors of Stromelysin Using SAR by NMR. *J. Am. Chem. Soc.*,
833 119, 5818 – 5827, DOI: 10.1021/ja9702778, 1997.

834 Hammond, M.C, Harris, B. Z., Lim, W. A., Bartlett, P. A.: β Strand Peptidomimetics as Potent PDZ
835 Domain Ligands. *Chem. Biol.*, 13(12), 1247-1251, DOI: 10.1016/j.chembiol.2006.11.010, 2006.

836 Harris, B. Z., Lau, F. W., Fujii, N., Guy, R. K. and Lim, W. A.: Role of electrostatic interactions in
837 PDZ domain ligand recognition. *Biochem.*, 42, 2797-2805, DOI: 10.1021/bi027061p, 2003.

838 Haugaard-Kedström, L. M., Clemmensen, L. S., Sereikaite, V., Jin, Z., Fernandes, E. F. A., Wind, B.,
839 Abalde-Gil, F., et al.: A High-Affinity Peptide Ligand Targeting Syntenin Inhibits Glioblastoma. *J.*
840 *Med. Chem.* 64(3), 1423-1434, DOI: 10.1021/acs.jmedchem.0c00382, 2021.

841 Hegedüs, Z., Hóbor, F., Shoemark, D. K., Celis, S., Lian, L.-Y., Trinh, Ch. H., Sessions, R. B.,
842 Edwards, T. A., Wilson, A. J.: Identification of β -strand mediated protein–protein interaction
843 inhibitors using ligand-directed fragment ligation. *Chem. Sci.*, 12, 2286, DOI: 10.1039/d0sc05694d,
844 2021.

845 Hillier, B. J., Christopherson, K. S., Prehoda, K. E., Bredt, D. S. and Lim, W. A.: Unexpected modes
846 of PDZ domain scaffolding revealed by structure of nNOS–syntrophin complex. *Science*, 284, 812–
847 815, 1999.

848 Holland, J. D., Klaus, A., Garratt, A. N. and Birchmeier, W.: Wnt signaling in stem and cancer stem
849 cells. *Curr. Opin. Cell Biol.*, 25, 254-264, DOI: 10.1016/j.ceb.2013.01.004, 2013.

850 Hori, K., Ajioky, K., Goda, N., Shindo, A., Tagagishi, M., Tenno, T. and Hiroaki, H.: Discovery of
851 Potent Dishevelled/Dvl Inhibitors Using Virtual Screening Optimized With NMR-Based Docking
852 Performance Index. *Front. Pharmacol.*, 9, 983, DOI: 10.3389/fphar.2018.00983, 2018.

853 Jain, A.K. and Dubes, R.C. Upper Saddle River, NJ: Prentice Hall, Algorithms for clustering data.
854 320p, 1988.

855 Jho, E. H., Zhang, T., Domon, C., Joo, C.-K., Freund, J.-N. and Costantini, F.: Wnt/beta-catenin/Tcf
856 signaling induces the transcription of Axin2, a negative regulator of the signaling pathway. *Mol.*
857 *Cell. Biol.*, 22, 1172 - 1183, DOI: 10.1128/mcb.22.4.1172-1183.2002, 2002.

858 Kanwar, S. S., Yu, Y., Nautyal, J., Patel, B. B. and Majumdar, A. P. N.: The Wnt/beta-catenin
859 pathway regulates growth and maintenance of colonospheres. *Mol. Cancer.*, 9, 212, DOI:
860 10.1186/1476-4598-9-212, 2010.

861 Kim, H. Y., Choi, S., Yoon, J. H., Lim, H. J., Lee, H., Choi, J., Ro, E. J., Heo, J. N., Lee, W., No, K.
862 T. and Choi, K. Y.: Small molecule inhibitors of the Dishevelled-CXXC5 interaction are new drug
863 candidates for bone anabolic osteoporosis therapy. *EMBO Mol. Med.*, 8, 375-387, DOI:
864 10.15252/emmm.201505714, 2016.

865 Klaus, A. and Birchmeier, W.: Wnt signalling and its impact on development and cancer. *Nat. Rev.*
866 *Cancer*, 8, 387-398, DOI: 10.1038/nrc2389, 2008.

867 Kurakin, A., Swistowski, A., Wu, S. C. and Bredesen, D. E.: The PDZ domain as a complex adaptive
868 system. *PLoS One*, 2(9), e953, DOI: 10.1371/journal.pone.0000953, 2007.

869 Lee, I., Choi, S., Yun, J. H., Seo, S. H., Choi, S., Choi, K. Y. and Lee, W.: Crystal structure of the
870 PDZ domain of mouse Dishevelled 1 and its interaction with CXXC5. *Biochem. Biophys. Res.*
871 *Commun.*, 485, 584-590, DOI: 10.1016/j.bbrc.2016.12.023, 2017.

872 Lee, H. J., Wang, N. X., Shi, D. L. and Zheng, J. J.: Sulindac inhibits canonical Wnt signaling by
873 blocking the PDZ domain of the protein dishevelled. *Angew. Chem. Int. Ed. Engl.*, 48, 6448 - 6452,
874 DOI: 10.1002/anie.200902981, 2009.

875 Lee, H. J., Wang, X. N., Shao, Y. and Zhenz, J. J.: Identification of tripeptides recognized by the PDZ
876 domain of Dishevelled. *Bioorg. Med. Chem.*, 17, 1701 – 1708, 2009. ,

877 Lewis, A., Segditsas, S., Deheragoda, M., Pollard, P., Jeffery, R., Nye, E., Lockstone, H., Davis, H.,
878 Clark, S., Stamp, G., Poulson, R., Wright, N. and Tomlinson, I.: Severe polyposis in Apc(1322T)
879 mice is associated with submaximal Wnt signalling and increased expression of the stem cell marker
880 Lgr5. *Gut.*, 59, 1680 - 1686, DOI: 10.1136/gut.2009.193680, 2010.

881 Lipinski, C. A.: Drug-like properties and the causes of poor solubility and poor permeability. *J.*
882 *Pharmacol. Toxicol. Meth.*, 44, 235 – 249 . DOI : 10.1016/s1056-8719(00)00107-6, 2000.
883 Lipinski, C. A., Lombardo, F., Dominy, B. W. and Feeney, P. J.: Experimental and computational
884 approaches to estimate solubility and permeability in drug discovery and development settings. *Adv.*
885 *Drug Deliv. Rev.*, 23, 3 – 25 . DOI : 10.1016/S0169-409X(96)00423-1, 1997.
886 Lv, P. C., Zhu, H. L., Li, H. Q., Sun, J. and Zho, Y.: Synthesis and biological evaluation of pyrazole
887 derivatives containing thiourea skeleton as anticancer. *Bioorg. Med. Chem.*, 18, 4606 - 4614, DOI:
888 10.1016/j.bmc.2010.05.034, 2010.
889 Madrzak, J., Fiedler, M. Johnson, Ch. et al.: Ubiquitination of the Dishevelled DIX domain blocks its
890 head-to-tail polymerization. *Nat. Commun.*, 6, 6718, DOI: 10.1038/ncomms7718, 2015.
891 Malanchi, I., Peinado, H., Kassen, D., Hussenet, T., Metzger, D., Chambon, P., Huber, M., Hohl, D.,
892 Cano, A., Birchmeier, W. and Huelsken, J.: Cutaneous cancer stem cell maintenance is dependent on
893 beta-catenin signalling. *Nature.*, 452, 650 - 653, DOI: 10.1038/nature06835, 2008.
894 Mathvink, R. J., Barritta, A. M., Candelore, M. R., Cascieri, M. A., Deng, L., Tota, L., Strader, C. D.,
895 Wyvratt, M. J., Fosher, M. H. and Weber, A. E.: Potent, elective human beta3 adrenergic receptor
896 agonists containing a substituted indoline-5-sulfonamide pharmacophore. *Bioorg. Med. Chem. Lett.*,
897 9, 1869 - 1874, DOI: 10.1016/s0960-894x(99)00277-2, 1999.
898 McCoy, A. J., Grosse-Kunstleve, R. W., Adams, P. D., Winn, M. D., Storoni, L. C. and Read, R. J.:
899 Phaser crystallographic software. *J. Appl. Cryst.*, 40(Pt4), 658 - 674, DOI:
900 10.1107/S0021889807021206, 2007.
901 McMartin, C. and Bohacek, R. S.: Powerful, rapid computer algorithms for structure-based drug
902 design, *J. Computer-Aided Mol. Des.*, 11, 333 – 344, DOI: 10.1023/a:1007907728892, 1997.
903 Mizutani, K., Miyamoto, S., Nagahata, T., Konishi, N., Emi, M. and Onda, M.: Upregulation and
904 overexpression of DVL1, the human counterpart of the Drosophila Dishevelled gene, in prostate
905 cancer. *Tumori*, 91, 546 – 551, 2005.
906 Molenaar, M., van de Wetering, M., Oosterweeggl, M., Peterson-Maduro, J., Godsave, S., Korinek,
907 V., Roose, J., Destrée, O. and Clevers, H.: XTcf-3 transcription factor mediates beta-catenin-induced
908 axis formation in Xenopus embryos. *Cell.*, 86, 391 - 399, DOI: 10.1016/s0092-8674(00)80112-9,
909 1996.
910 Mosmann, T.: Rapid colorimetric assay for cellular growth and survival: application to proliferation
911 and cytotoxicity assays. *J. Immunol. Methods.*, 65, 55 - 63, DOI: 10.1016/0022-1759(83)90303-4,
912 1983.
913 Murshudov, G. N., Vagin, A. A. and Dodson, E. J.: Refinement of macromolecular structures by the
914 maximum-likelihood method. *Acta Cryst.*, 53, 240 - 255, DOI: 10.1107/S0907444996012255, 1997.
915 O'Brien, P. M., Ortwine, D. F., Pavlovsky, A. G., Picard, J. A., Sliskovic, D. R., Roth, B. D., Dyer, R.
916 D., Johnson, L. L., Man, C. F. and Hallak, H.: Structure-activity relationships and pharmacokinetic
917 analysis for a series of potent, systemically available biphenylsulfonamide matrix metalloproteinase
918 inhibitors. *J. Med. Chem.*, 43, 156 - 166, DOI: 10.1021/jm9903141, 2000.
919 Osada, R., Funkhouser, T., Chazelle, D. and Dobkin, D.: Shape distributions, *ACM Transactions on*
920 *Graphics*, 21(4), 807 – 832, DOI: 10.1145/571647.571648, 2002
921 Pawson, T.: Dynamic control of signalling by modulator adaptor proteins. *Curr. Opin. Cell Biol.*, 19,
922 112 -116, DOI: 10.1016/j.ceb.2007.02.013, 2007.
923 Polakis, P.: Drugging Wnt signaling in cancer. *EMBO J.*, 31, 2737-2746, DOI:
924 10.1038/emboj.2012.126, 2012.
925 Ponting, C. P., Phillips, C., Davies, K. E. and Blake, D. J.: PDZ domains: targeting signalling
926 molecules to submembranous sites. *Bioassays*, 19, 469 – 479, DOI: 10.1002/bies.950190606, 1997.
927 Puranik, P., Aakanksha, K., Tadas, S. V., Robert, D. B., Lalji, K. G. and Vincent, C. O. N.: Potent
928 anti-prostate cancer agents derived from a novel androgen receptor down-regulating agent. *Bioorg.*
929 *Med. Chem.*, 16, 3519 – 3529, DOI: 10.1016/j.bmc.2008.02.031, 2008.
930 Qin, Y., Feng, L., Fan, X., Zheng, L., Zhang, Y., Chang, L., Li, T.: Neuroprotective Effect of N-
931 Cyclohexylethyl-[A/G]-[D/E]-X-V Peptides on Ischemic Stroke by Blocking nNOS–CAPON
932 Interaction. *ACS Chem. Neurosci.* 12(1), 244-255, DOI: 10.1021/acschemneuro.0c00739, 2021.
933 Riese, J., Yu, X., Munnerly, A., Eresh, L., Hsu, S.-C., Grosschedl, R. and Bienz, M.: LEF-1, a nuclear
934 factor coordinating signaling inputs from wingless and decapentaplegic. *Cell*, 88, 777 - 787, DOI:
935 10.1016/s0092-8674(00)81924-8, 1997.

936 Rimbault, C., Maruthi, K., Breillat, C., Genuer, C., Crespillo, S., Puente-Muñoz, V., Chamma, I.,
937 Gauthereau, I., Antoine, S., Thibaut, C., Tai, F. W. J., Dartigues, B., Grillo-Bosch, D., Claverol, S.,
938 Poujol, C., Choquet, D., Mackereth, C. D. and Sainlos, M.: Engineering selective competitors for the
939 discrimination of highly conserved protein-protein interaction modules. *Nat. Commun.*, 10, 4521,
940 DOI: 10.1038/s41467-019-12528-4, 2019.

941 Sack, U., Walther, W., Scudiero, D., Selby, M., Aumann, J., Lemos, C., Fichtner, I., Schlag, P. M.,
942 Shoemaker, R. H. and Stein, U.: S100A4-induced cell motility and metastasis is restricted by the
943 Wnt/beta-catenin pathway inhibitor calcimycin in colon cancer cells. *Mol. Biol. Cell.*, 22, 3344 -
944 3354, DOI: 10.1091/mbc.E10-09-0739, 2011.

945 Sanner, M. F., Olson, A. J. and Spehner, J. C.: Reduced surface: an efficient way to compute molecular
946 surfaces, *Biopolymers*, 38, 305 – 320, DOI: 10.1002/(SICI)1097-0282(199603)38:3%3C305::AID-
947 BIP4%3E3.0.CO;2-Y, 1996.

948 Saupe, J., Roske, Y., Schillinger, C., Kamdem, N., Radetzki, S., Diehl, A., Oschkinat, H., Krause, G.,
949 Heinemann, U. and Rademann, J.: Discovery, structure-activity relationship studies, and crystal
950 structure of non-peptide inhibitors bound to the Shank3 PDZ domain. *ChemMedChem*, 6, 1411 -
951 1422, DOI: 10.1002/cmcd.201100094, 2011.

952 Schultz, J., Hoffmüller, U., Krause, G., Ashurts, J., Macias, M. J., Schmieder, P., Schneider-Mergener,
953 J. and Oschkinat, H.: Specific interactions between the syntrophin PDZ domain and voltage-gated
954 sodium channels. *Nat. Struct. Biol.*, 5, 19 – 24, DOI: 10.1038/nsb0198-19, 1998.

955 Schwarz-Romond, T., Fiedler, M., Shibata, N., Butler, P.J.G., Kikuchi, A., Higuchi, Y., Bienz, M.:
956 The DIX domain of Dishevelled confers Wnt signaling by dynamic polymerization. *Nat. Struct. Mol.*
957 *Biol.*, 14(6), 484-492, DOI: 10.1038/nsmb1247, 2007.

958 Shan, J., Shi, D. L., Wang, J. and Zheng, J.: Identification of a specific inhibitor of the dishevelled
959 PDZ domain. *Biochem.*, 44, 15495-15503, DOI: 10.1021/bi0512602, 2005.

960 Shan, J., Zhang, X., Bao, J., Cassell, R. and Zheng, J. J.: Synthesis of potent Dishevelled PDZ domain
961 inhibitors guided by virtual screening and NMR studies, *Chem. Biol. Drug. Des.*, 79, 376 – 383,
962 DOI: 10.1111/j.1747-0285.2011.01295.x, 2012.

963 Sheng, M. and Sala, C.: PDZ domains and the organization of supramolecular complexes. *Annu. Rev.*
964 *Neurosci.*, 24, 1 – 29, DOI: 10.1146/annurev.neuro.24.1.1, 2001.

965 Sievers, F., Wilm, A., Dineen, D. G., Gibson, T. J., Karplus, K., Li, W., Lopez, R., McWilliam, H.,
966 Remmert, M., Söding, J., Thompson, J. D. and Higgins, D. G.: Fast, Scalable generation of high-
967 quality protein multiple sequence alignments using Clustal Omega. *Mol. Syst. Biol.*, 7, 539,
968 Doi:10.1038/msb.2011.75, 2011.

969 Sineva, G. S. and Pospelov, V. A.: Inhibition of GSK3beta enhances both adhesive and signalling
970 activities of beta-catenin in mouse embryonic stem cells. *Biol. Cell*, 102, 549-560, DOI:
971 10.1042/BC20100016, 2010.

972 Sleight, A. J., Boess, F. G., Bös, M., Levet-Trafit, B., Riemer, C. and Bourson, A. Br.:
973 Characterization of Ro 04-6790 and Ro 63-0563: potent and selective antagonists at human and rat
974 5-HT6 receptors. *J. Pharmacol.*, 124, 556 - 562, DOI: 10.1038/sj.bjp.0701851, 1998.

975 Songyang, Z., Fanning, A. S., Fu, C., Xu, J., Marfatia, S. M., Chisti, A. H., Crompton, A., Chan, A.
976 C., Anderson, J. M. and Cantley, L. C.: Recognition of unique carboxyl-terminals motifs by distinct
977 PDZ domains. *Science*, 275, 73 - 77, DOI: 10.1126/science.275.5296.73, 1997.

978 Shuker, S. B., Hajduk, P. J., Meadows, R. P. and Fesik, S. W.: Discovering high-affinity ligands for
979 proteins: SAR by NMR. *Science*, 274, 1531 – 1534, DOI: 10.1126/science.274.5292.1531, 1996.

980 Shuker, S. B., Hajduk, P. J., Meadows, R. P. and Fesik, S. W.: Discovering high-affinity ligands for
981 proteins: SAR by NMR. *Science*, 274, 1531 – 1534, DOI: 10.1126/science.274.5292.1531, 1996.

982 Tellew, J. E., Baska, R. A. F., Beyer, S. M., Carlson, K. E., Cornelius, L. A., Fadnis, L., Gu, Z., Kunst,
983 B. L., Kowala, M. C., Monshizadegan, H., Murugesan, N., Ryan, C. S., Valentine, M. T., Yang, Y.
984 and Macor, J. E.: Discovery of 4-[(imidazol-1-yl)methyl]biphenyl-2-sulfonamides as dual
985 endothelin/angiotensin II receptor antagonists. *Bioorg. Med. Chem. Letters*, 13, 1093 – 1096, DOI:
986 10.1016/s0960-894x(03)00018-0, 2003.

987 [The PyMOL Molecular Graphics System, Version 2.3.4 Schrödinger, LLC](#)

988 Uematsu, K., He, B., You, L., Xu, Z., McCormick, F. and Jablons, D. M.: Activation of the Wnt
989 pathway in non-small cell lung cancer: evidence of dishevelled overexpression. *Oncogene*, 22, 7218
990 - 7221, DOI: 10.1038/sj.onc.1206817, 2003.

991 Uematsu, K., Kanazawa, S., You, L., He, B., Xu, Z., Li, K., Peterlin, B. M., McCormick, F. and
992 Jablons, D. M.: Wnt pathway activation in mesothelioma: evidence of dishevelled overexpression and
993 transcriptional activity of β -catenin. *Cancer Res.*, 63, 4547 – 4551, 2003.

994 Vermeulen, L., De Sousa E Melo, F., van der Heijden, M., Cameron, K., de Jong, J. H., Borovski, T.,
995 Tuynman, J. B., Todaro, M., Merz, C., Rodermond, H., Sprick, M. R., Kemper, K., Richel, J. J.,
996 Stassi, G. and Medema, J. P.: Wnt activity defines colon cancer stem cells and is regulated by the
997 microenvironment. *Nat. Cell. Biol.*, 12, 468 - 476, DOI: 10.1038/ncb2048, 2010.

998 Wallingford, B. J. and Raymond H.: The developmental biology of Dishevelled: an enigmatic protein
999 governing cell fate and cell polarity. *Development*, 132, 4421 - 4436, DOI: 10.1242/dev.02068,
1000 2005.

1001 Wang, C., Dai, J., Sun, Z., Shi, C., Cao, H., Chen, X., Gu, S., Li, Z., Qian, W. and Han, X.: Targeted
1002 inhibition of dishevelled PDZ domain via NSC668036 depresses fibrotic process. *Exp. Cell Res.*,
1003 331, 115 – 122, DOI: 10.1016/j.yexcr.2014.10.023, 2015.

1004 Weeraratna, A. T., Jiang, Y., Hostetter, G., Rosenblatt, K., Duray, P., Bittner, M. and Trent, J. M.:
1005 Wnt5a signalling directly affects cell motility and invasion of metastatic melanoma. *Cancer Cell*, 1,
1006 279 – 288, DOI: 10.1016/s1535-6108(02)00045-4, 2002.

1007 Wong, H. C., Bourdelas, A., Krauss, A., Lee, H. J., Shao, Y., Wu, D., Mlodzik, M., Shi, D. L. and
1008 Zheng, J.: Direct binding of the PDZ domain of Dishevelled to a conserved internal sequence in the
1009 C-terminal region of Frizzled J. *Mol. Cell*, 12, 1251 -1260, DOI: 10.1016/s1097-2765(03)00427-1,
1010 2003.

1011 Wong, H., Mao, J., Nguyen, J. T., Srinivas, S., Zhang, W., Liu, B., Li, L., Wu, D. and Zheng, J.:
1012 Structural basis of the recognition of the dishevelled DEP domain in the Wnt signalling pathway.
1013 *Nat. Struct. Biol.*, 7, 1178 -1184, DOI: 10.1038/82047, 2000.

1014 Wu, C., Decker, E. R., Blok, N., Bui, H., Chen, Q., Raju, B., Bourgoyne, A. R., Knowles, V.,
1015 Biediger, R. J., Market, R. V., Lin, S., Dupre, B., Kogan, T. P., Holland, G. W., Brock, T. A. and
1016 Dixon, R. A. F.: Endothelin antagonists: substituted mesitylcarboxamides with high potency and
1017 selectivity for ET(A) receptors. *J. Med. Chem.*, 42, 4485 - 4499, DOI: 10.1021/jm9900063, 1999.

1018 Zartler, E. R. and Shapiro, M. J.: Protein NMR-based screening in drug discovery. *Curr. Pharm. Des.*,
1019 12, 3963 – 3972, DOI: 10.2174/138161206778743619, 2006.

1020 Zartler, E. R., Hanson, J., Jones, B. E., Kline, A. D., Martin, G., Mo, H., Shapiro, M. J., Wang, R.,
1021 Wu, H. and Yan, J.: RAMPED-UP NMR: multiplexed NMR-based screening for drug discovery. *J.*
1022 *Am. Chem. Soc.*, 125, 10941 - 10946, DOI: 10.1021/ja0348593, 2003.

1023 Zhang, M. and Wang, W.: Organization of signalling complexes by PDZ-domain scaffold proteins.
1024 *Acc. Chem. Res.*, 36, 530 – 538, DOI: 10.1021/ar020210b, 2003.

1025 Zhang, M. and Wang, W.: Organization of signalling complexes by PDZ-domain scaffold proteins.
1026 *Acc. Chem. Res.*, 36, 530 – 538, DOI: 10.1021/ar020210b, 2003.

1027 Zhang, Y., Appleton, B. A., Wiesmann, C., Lau, T., Costa, M., Hannoush, R. N. and Sidhu, S. S.:
1028 Inhibition of Wnt signaling by Dishevelled PDZ peptides. *Nat. Chem. Biol.*, 5, 217 -219, DOI:
1029 10.1038/nchembio.152, 2009.